62 72282 Copy 634

[redacted]

NASA TM X-458

NASA TM X-458

[redacted]

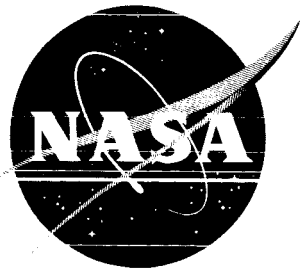

CASE FILE COPY

TECHNICAL MEMORANDUM

X-458

Declassified by authority of NASA
Classification Bulletin Notices No. 43
Dated 6-25-62

MEASUREMENTS OF THE SURFACE FLOWS, HEAT TRANSFER, PRESSURE DISTRIBUTION, AND LONGITUDINAL STABILITY OF A MERCURY CAPSULE MODEL AT MACH NUMBERS OF 6.9 AND 9.6

By Philip E. Everhart and Peter T. Bernot

Langley Research Center
Langley Field, Va.

[redacted]

NATIONAL AERONAUTICS AND SPACE ADMINISTRATION

WASHINGTON

April 1961

[redacted]

1B

DECLASSIFIED

NATIONAL AERONAUTICS AND SPACE ADMINISTRATION

TECHNICAL MEMORANDUM X-458

MEASUREMENTS OF THE SURFACE FLOWS, HEAT TRANSFER, PRESSURE DISTRIBUTION, AND LONGITUDINAL STABILITY OF A MERCURY CAPSULE MODEL AT MACH NUMBERS OF 6.9 AND 9.6*

By Philip E. Everhart and Peter T. Bernot

SUMMARY

An investigation of the pressure distribution and heat transfer on a 0.03-scale model of the Mercury capsule reentry configuration has been made in the Langley 11-inch hypersonic tunnel at a Mach number of 9.6, a Reynolds number of 240,000 based on maximum model diameter and an angle-of-attack range from 0° to 15°. Schlieren and oil-flow studies of the flow field about the capsule were made at Mach numbers of 6.9 and 9.6. The results at a Mach number of 9.6 indicated that, in general, the local heating rates on the afterbody are less than 10 percent of the stagnation-point heating rate throughout the angle-of-attack range of the investigation, and the pressures on the afterbody were less than 4 percent of the pressure on the capsule face. At angle of attack the heating rates generally decreased with circumferential distance from the windward side. The method of N. H. Kemp and F. R. Riddell of the AVCO Research Laboratory, modified for a spherical segment as shown by W. S. Stoney in NACA RM L58E05a, and a modified Sibulkin theory, using a nondimensional velocity gradient calculated from data obtained on a 1/7-scale model of the Mercury capsule, show good agreement with the experimental stagnation-point heating rate at an angle of attack of 0°. The variation in Stanton number with angle of attack was small on the forward face but was considerably larger on the afterbody.

The static stability tests at a Mach number of 9.6 of the escape, exit, and reentry versions of the Mercury capsule indicated that all configurations exhibited positive static stability characteristics and that the exit version had the lowest degree of stability.

*Title, Unclassified.

[redacted]

[redacted]

INTRODUCTION

A brief review of the scope of the wind-tunnel studies which have been made on Project Mercury is given in reference 1. The Mercury capsule is a manned, nonlifting ballistic vehicle capable of orbital flight and safe reentry. The basic configuration was selected after an extensive study of shapes which not only would minimize the reentry heating problem but also would satisfy numerous stability requirements. The basic capsule has a blunt reentry face, a conical afterbody, and a tower-like structure which provides for escape in the event of an aborted flight. The exit version has the conical section forward and the reentry version has the blunt end forward. After successful launching the escape system is to be jettisoned in order to reduce the weight prior to insertion into orbit. At insertion into orbit the capsule is intended to separate from the booster and to orbit with the blunt hemispherical face forward. After several orbits are completed, the capsule velocity is reduced and reentry begins.

L 1220

The research and development program being conducted in support of the NASA Project Mercury has been conceived to yield experimental data necessary to an efficient capsule design as well as to provide data for all phases of the operational aspects of the project. Numerous wind-tunnel tests have been conducted to investigate the aerodynamic behavior and heating of the capsule in the Mach number range from 0 to 20 (for example, refs. 2 to 5). Models ranging from as small as 0.01 full scale to full scale have been used. As part of this program a 0.03-scale model of the Mercury capsule reentry configuration has been tested in the Langley 11-inch hypersonic blowdown wind tunnel at a Mach number of 9.6 and at a Reynolds number (based on model maximum diameter) of 0.24×10^6 to obtain aerodynamic heating and pressure data at angles of attack from 0° to 15°. Some flow visualization data were obtained in this tunnel at Mach numbers of 6.9 and 9.6.

A static stability investigation of the escape, exit, and reentry versions of the Mercury capsule was also conducted at a Mach number of 9.6 and a Reynolds number based on model maximum diameter of 0.14×10^6. A strain-gage balance was employed to measure normal and axial forces as well as pitching moments over an angle-of-attack range from -4° to 25°.

SYMBOLS

All forces and moments are referenced to body-axis system. (See fig. 1.)

[redacted]

DECLASSIFIED

A	reference area based on maximum body diameter, sq in.
a_t	speed of sound at stagnation temperature, ft/sec
C_A	axial-force coefficient, F_A/qA
C_m	pitching-moment coefficient, M_Y/qAd
C_{m_α}	slope of pitching-moment-coefficient curve, per deg
C_N	normal-force coefficient, F_N/qA
C_{N_α}	slope of normal-force-coefficient curve, per deg
c_p	free-stream specific heat at constant pressure, Btu/lb-$^\circ$R
d	maximum body diameter, in.
F_A	corrected axial force, lb
F_N	normal force, lb
h	heat-transfer coefficient, Btu/ft^2-sec-$^\circ$R
M	free-stream Mach number
M_Y	pitching moment, in-lb
N_{St}	Stanton number based on free-stream static conditions, $h/\rho c_p u$
p	static pressure on model surface, lb/sq in.
p_t	supply pressure, lb/sq in.
N_{Pr}	Prandtl number, 0.72
q	local heat-transfer rate, Btu/ft^2-sec; also, dynamic pressure, lb/sq in.
q_1	heat-transfer rate measured by the thermocouple on the axis of symmetry, Btu/ft^2-sec
r	radial distance from capsule axis of symmetry, in.

[redacted]

r_{max}	maximum body radius, in.
R_d	free-stream Reynolds number based on model maximum diameter
R_s	Reynolds number based on wetted distance
s	wetted distance measured from stagnation point, in.
t_{aw}, T_{aw}	adiabatic wall temperature, ^{o}F and ^{o}R, respectively
t_t, T_t	stagnation temperature, ^{o}F and ^{o}R, respectively
t_l, T_l	local static temperature, ^{o}F and ^{o}R, respectively
t_w	wall temperature, ^{o}F
u	free-stream flow velocity, ft/sec
α	angle of attack referenced from model center line, deg
η_r	temperature recovery factor, $\sqrt{N_{Pr}}$
ρ	free-stream air density, lb/cu ft
ϕ	meridian angle, deg

APPARATUS AND TESTS

This investigation was conducted in the Langley 11-inch hypersonic tunnel. This blowdown wind tunnel operates intermittently at an average Mach number of 9.6. A description of the tunnel may be found in reference 6 and the pressure distributions in the three-dimensional nozzle are presented in reference 7. The central core of uniform flow for the three-dimensional nozzle measures about 4 inches in both the vertical and the horizontal directions with a variation in Mach number and pressure as indicated in reference 7. The stagnation temperature was maintained at an average value of 1,200° F by means of a variable-frequency, resistance-tube heater to insure against liquefaction of the air. The heat-transfer and surface-pressure tests were made at a stagnation pressure of approximately 47 atmospheres and the stability tests at a supply pressure of 27 atmospheres giving Reynolds numbers based on the model maximum diameter (2.25 in.) about 0.24×10^6 and 0.14×10^6.

The 0.03-scale heat-transfer model of the Mercury capsule was made of 1020 steel, 0.072 inch thick on the hemispherical face and 0.010 inch thick on the conical afterbody. The model was mounted on a support structure attached to the floor of the tunnel as shown in figure 2(a), and changes in angle of attack were accomplished by installing wedges at

[redacted]

DECLASSIFIED

the base of the support structure. Model dimensions with pressure and thermocouple locations are given in figure 2(b). Heat-transfer and pressure measurements were obtained on both the forward face and the afterbody. The thermocouples were No. 30 chromel-alumel wire and were fastened to the model by welding a preformed bead into a hole drilled through the skin. Continuous records of the stagnation temperature and the capsule skin temperatures were obtained on 18-channel recording galvanometers. The pressure orifices were located diametrically opposite their corresponding thermocouple locations and the model was tested through an angle-of-attack range from -15° to $+15^{\circ}$ in order to obtain pressure and heat-transfer data on both surfaces of the body. The stagnation and orifice pressures on the model were recorded on NASA aneroid-type six-cell recording units described in reference 6. An accuracy of approximately 1/2 of 1 percent of full-scale deflection can be obtained on the low-pressure instruments through careful calibration and reading of the records. For this investigation pressure cells were chosen to give as near full-scale deflection as possible for the measuring station.

The force-test models used in the stability investigation were also built to a 0.03 scale. Photographs of the escape, exit, and reentry configurations are shown in figures 3(a), 3(b), and 3(c), respectively. Model details are presented in figure 3(d). A sting-mounted strain-gage balance was employed to measure normal and axial forces as well as pitching moments. Circular metal shields were used to protect the exposed portions of the balances behind the models. Base pressures were obtained by taping a 1/8-inch metal tube to the shield and employing an ionization gage to measure the pressure. The measured axial forces were adjusted so that the coefficients represent values for a model with free-stream static pressure acting on the base.

On the basis of calibrations and previous experience, estimations of maximum errors of the measured stability parameters are presented, as follows:

Configurations	C_N	C_A	C_m	α, deg
Escape version	±0.026	±0.008	±0.026	±0.20
Exit version	±.026	±.008	±.011	±.20
Reentry version	±.026	±.008	±.027	±.20

On the basis of previous experience the accuracy of the heat-transfer data varies, in general, between 10 and 20 percent.

In order to visualize the flow patterns at the surface of the model two oil-flow techniques were used in this investigation. The first

method consisted of completely coating the model with a mixture of oil and lampblack. The second method consisted of applying the mixture of lampblack and oil to the model in a dot pattern. The dot method was used in most of these tests.

The schlieren system used in these tests had a single-pass vertical Z light path with a horizontal knife edge. The light source for the schlieren photographs was a mercury vapor arc lamp having a duration of about 3 microseconds.

RESULTS AND DISCUSSION

A summary of the pertinent heat-transfer and surface-pressure results is presented in table I. Values of Reynolds number and Stanton number are based on free-stream conditions. Reynolds number R_s in table I incorporates the wetted distance from the stagnation point as the characteristics length. The temperature data were reduced according to the method given in reference 8. The adiabatic wall temperatures used to reduce the heat-transfer data, shown in table I, are estimated values. These estimated values were obtained from the following equation:

$$\frac{T_{aw}}{T_t} = \left(1 - \eta_r\right)\frac{T_l}{T_t} + \eta_r$$

with T_l/T_t obtained from the local Mach number using the measured pressures and an average recovery factor η_r assumed for the entire model including both attached and separated flows. This assumed value was $\eta_r = \sqrt{N_{Pr}} = 0.848$. (See ref. 9.)

Typical schlieren photographs of the capsule at various angles of attack are presented in figure 4 for a Mach number of 9.6 and in figure 5 for a Mach number of 6.9. In order to supplement the schlieren flow study, oil-flow tests were made at Mach numbers of 9.6 and 6.9 and Reynolds numbers of 0.24×10^6 and 0.68×10^6, respectively, for various angles of attack on the floor-mounted model and on a sting-mounted model. The data are presented in figures 6, 7, and 8.

Figure 4(a) presents the model at $\alpha = 0^\circ$, and it can be seen that the bow shock is deflected by the tunnel boundary layer. The shock standoff distance is approximately 4 percent smaller than that of a body of revolution with a flat nose (ref. 10) having the same diameter as the

DECLASSIFIED

diameter of the capsule. The shock about the model at angles of attack of 5° and 10° is presented in figures 4(b) and 4(c). Although the capsule shoulder came very close to the tunnel boundary layer at an angle of attack of 10° (fig. 4(c)), it is believed that the data in this region are valid. It can be seen from figure 4(d) that at $\alpha = 15°$, the capsule nose shock causes the tunnel-wall boundary layer to separate and strike the model nose and thus to invalidate any data obtained for this condition. The shock about the capsule at negative angles of attack is presented in figures 4(e), 4(f), and 4(g). Because of the geometry of the support system, the model was raised higher above the tunnel center line when the wedges were used to increase angle of attack than it was lowered below the center line when the wedges for negative angles of attack were used. At $\alpha = -15°$ the model was far enough away from the tunnel wall to prevent disturbances in the tunnel-wall boundary layer which would affect the model, and the data obtained at this condition are valid.

Very little detail of the afterbody flow field is apparent in the photographs because of the extremely low density in this region at M = 9.6. In order to make a more detailed study of the flow field in the region of the afterbody, additional schlieren tests were conducted on a sting-mounted model at a Mach number of 6.9 (fig. 5). At $\alpha = 0°$ (fig. 5(a)) the flow separates a short distance from the juncture of the nose and the cone and reattaches on the cylindrical section. This reattachment creates a weak shock on the cylinder. A second separation and reattachment occurs on the canister. The separations and reattachments are also shown in the oil-flow photographs at a Mach number of 6.9 and 9.6 in figures 6(a), 7(a), 7(b), and 8(a). The lines shown in the region of separation on the cone in figure 7(a) are not flow lines but are merely brush marks created in applying a more or less uniform coating of the oil solution. The dot traces in figure 7(b) show low shear stress on the cone as compared with that in the region just behind the corner and thus indicate separation. The angle of separation measured from the oil-flow photograph (fig. 7(a)) was 17.25° from the free-stream direction as compared with an angle of 16.5° measured from the schlieren photograph (fig. 5(a)). The schlieren photographs indicate that at angles of attack (figs. 5(b), 5(c), and 5(d)), weak shocks are generated on the windward side of the model where changes in surface slope occur and that the leeward side of the model seems to be blanketed by the separated flow. The oil-flow photographs show that separated flow exists on the conical section of the capsule up to $\alpha = 10°$. (See figs. 7(c) and 7(d).) Note the interference effect of the flow around the side mount over parts of the cylinder and canister (fig. 6).

The front-view photographs of the oil patterns in figures 6, 7, and 8 show the location of the stagnation point on the capsule face for the angle-of-attack range. The variation of the stagnation point with angle

[redacted]

of attack for Mach numbers of 6.9 and 9.6 is plotted in figure 9. For the entire angle-of-attack range the stagnation point measured from the oil-flow study at a Mach number of 6.9 is only about 80 percent of the distance from the center of the model to the geometric stagnation point. At a Mach number of 9.6 the measured stagnation point shows good agreement with the geometric stagnation point for angles of attack up to about 5°. Beyond $\alpha = 5^\circ$, however, the measured stagnation point lags the geometric stagnation point and at $\alpha = 20^\circ$ is only 84 percent of the distance from the center of the model to the geometric stagnation point.

The experimental pressure distribution over the capsule is presented in figure 10 and indicates very little variation in the pressure near the shoulder on the capsule face with angle of attack. On the conical portion the pressure increases with distance on the windward side and 90° stations of the capsule (see figs. 10(a), 10(b), and 10(c)) but is more nearly constant on the leeward side (negative values of s/d in figs. 10(a) and 10(b)) for the angles of attack of the tests. The pressures on the afterbody were less than 4 percent of the pressure on the capsule face except for a few points on the canister at the 45° and 90° stations (see figs. 10(b) and 10(c)). At $\alpha = 0^\circ$ there is some variation in the pressures at the 45° and 90° stations on the cylinder and canister. This variation may be due to an interference effect of the flow around the floor mount over parts of the cylinder and canister as shown by the oil-flow streamlines in figure 6(a).

The variation of the ratio of the local heating rates to the heating rate measured by the thermocouple on the axis of symmetry with the wetted distance from the center of the forward face nondimensionalized with respect to maximum body diameter, s/d is presented in figure 11 for various angles of attack. As would be expected, the local heating-rate ratios q/q_1 on the forward face were much larger than those on the afterbody. In general, the local heating rates on the afterbody were found to be less than 10 percent of the stagnation heating rate throughout the angle-of-attack range. At angle of attack the heating rates generally decreased with circumferential distance from the windward side. The data indicate that the heating rate immediately behind the nose-cone juncture is approximately twice the heating rate on the rest of the cone. The oil-flow tests indicate that this thermocouple is in a region of attached flow. From figures 11(a) and 11(b) it can be seen that the heating rate on the afterbody drops sharply until about midway on the cone where it begins to increase rapidly over the remainder of the afterbody. This effect on the afterbody decreases as the angle of attack increases (figs. 11(c) and 11(d)) until at $\alpha = 15^\circ$ the heating rate on the afterbody appears to be fairly constant. The heating rates on the canister and the cylinder are higher than the heating rates over the rearward portion of the cone. These higher heating rates may be the

L 1220

[redacted]

DECLASSIFIED

result of the shock wave on the cylinder formed by the separation from the nose-cone juncture reattaching on the cylinder.

Two methods were used to estimate the stagnation-point heating rate. First, the method of Kemp and Riddell (ref. 11) was applied to the present geometry by using the modification for a spherical segment as shown by Stoney in reference 12. Secondly, a modified Sibulkin theory (ref. 13) and a nondimensional velocity gradient $\left(\frac{d(u/a_t)}{d(s/d)} = 1.285\right)$ calculated from data obtained on a 1/7-scale model of the Mercury capsule in the Langley Unitary Plan wind tunnel at a Mach number of 3.5 was used. Both methods predicted a stagnation-point heating-rate value of 8.7 Btu/ft^2-sec which compared favorably with an experimental stagnation-point heating-rate value of 9.4 $\pm$ 0.1 Btu/ft^2-sec.

The distribution of the Stanton number along the model is presented in figure 12. In general, the Stanton numbers on the afterbody were less than about 10 percent of those on the forward face throughout the angle-of-attack range. Using a modified Sibulkin theory (ref. 13) and the nondimensional velocity gradient of 1.285 mentioned previously gave good agreement with the experimental Stanton numbers on the forward face. (See fig. 12(a).) The variation in Stanton number with angle of attack is small for the stations on the front face, whereas there is a considerable increase in the Stanton number on the afterbody for the station $\phi = 0^\circ$ with increasing angle of attack (fig. 12(a)). Variation in Stanton number for the stations $\phi = 45^\circ$ and 90° is presented in figures 12(b) and 12(c). An increase in angle of attack brought about an appreciable decrease in Stanton number on the leeward side of the afterbody (negative s/d values in figs. 12(b) and 12(c)).

A simple approach was used to estimate the heat transfer to the afterbody of the capsule. The afterbody was treated as part of a flat plate with the origin of the flow at the stagnation point of the capsule, with the sonic point normal to the shoulder, and the pressure was calculated for the full expansion around the corner. The results of this calculation utilizing the flat-plate theory (ref. 14) are shown in figure 12(a) for $\alpha = 0^\circ$ and 15°. When the effect on the pressure of the decrease in the effective expansion angle caused by separation (as shown in figs. 7(a) and 7(b)) is taken into account, the calculated heat transfer is changed by only about 5 percent. However, with separation it might seem reasonable to apply Chapman's results (ref. 9), which indicate that the rate of heat transfer to a separated laminar region averages about 56 percent of a corresponding attached laminar boundary layer having the same constant pressure. With the 56-percent value taken as an invariant, the dashed line in figure 12(a) is obtained. Even this line is, in general, considerably above the data for $\alpha = 0^\circ$.

The longitudinal static stability results of the escape (tower on) and exit (tower off) versions of the Mercury capsule are presented in

[redacted]

figure 13. Both versions exhibit positive static stability characteristics up to an angle of attack of about 7°; however, the exit version has a much lower stability level. It should be mentioned here that the realistic center-of-gravity locations are different for each configuration. As angle of attack is increased, a condition of neutral stability is indicated near 8.5°, and then pitch-up tendencies are observed. Unfortunately, the length of the escape-version model precluded the testing at angles of attack greater than 11°.

As would be expected, the escape version displays a sizable reduction in axial-force coefficient since the escape tower acts in effect as a drag-reducing spike. It is to be noted that the axial-force coefficient is lower at $\alpha = \pm 2^\circ$ than at 0°. This effect is probably due to the unsymmetrical geometry of the escape tower and rocket nozzles. Unpublished data for this same model at a Mach number of 6.8 show the same trend. The higher level of normal-force coefficient for the escape version is to be expected since this configuration has a higher fineness ratio than the exit version.

The longitudinal characteristics of the reentry version are presented in figure 14. Positive static stability is indicated throughout the angle-of-attack range of these tests. The maximum axial-force coefficient obtained in these tests was 1.50 at $\alpha = 0^\circ$. The low values of normal-force coefficient are typical for configurations of this type (ref. 15).

A summary of stability parameters of the three versions of the Project Mercury capsule is as follows:

Configurations	$(C_{N_\alpha})_{\alpha=0^\circ}$	$(C_{m_\alpha})_{\alpha=0^\circ}$	$(C_A)_{\alpha=0^\circ}$
Escape version	0.040	-0.008	0.18
Exit version	.019	-.001	.25
Reentry version	.005	-.003	1.50

Schlieren photographs taken during the stability tests of the three capsule configurations at a Mach number of 9.6 are presented in figure 15. For the escape and exit versions, it is estimated that the bow shock starts to impinge on the capsule conical surface at an angle of attack of about 7°.

[redacted]

DECLASSIFIED

CONCLUDING REMARKS

An investigation has been made at a Mach number of 9.6 to obtain aerodynamic heating and pressure data on a 0.03-scale model of the Mercury capsule reentry configuration. The Reynolds number of the flow based on free-stream conditions and the model maximum diameter was approximately 0.24×10^6. Schlieren and oil-flow data were obtained at Mach numbers of 6.9 and 9.6 in order to study the capsule flow fields. Static longitudinal stability tests on the escape, exit, and reentry capsule configurations were made at a Mach number of 9.6 and a Reynolds number of 0.14×10^6.

L
1
2
2
0

Analysis of the experimental data obtained from these tests leads to the following conclusions:

1. The stagnation point heating rate could be reasonably well predicted by the method of Kemp and Riddell, in which a modification for a spherical segment as shown by Stoney was used, and by a modified Sibulkin theory with a nondimensional velocity gradient calculated from data obtained on a 1/7-scale model of the Mercury capsule. The variation in Stanton number with angle of attack was small for the forward face.

2. The Stanton number on the afterbody of the capsule varied considerably with angle of attack. At angle of attack the heating rates generally decreased with circumferential distance from the windward side. Heating rates on the windward side of the afterbody were shown to increase with angle of attack up to about 10 percent of the stagnation heating rate.

3. For the entire angle-of-attack range the stagnation point measured from the oil-flow study at a Mach number of 6.9 is only about 80 percent of the distance from the center of the model to the geometric stagnation point. The measured stagnation point for a Mach number of 9.6 was found to show good agreement with the geometric stagnation point for angles of attack up to 5°. At angles of attack beyond 5° the measured stagnation point lags the geometric stagnation point and at an angle of attack of 20° is only 84 percent of the distance from the center of the model to the geometric stagnation point.

4. The oil-flow tests at Mach numbers of 6.9 and 9.6 showed that the flow separated a short distance behind the nose-cone juncture and reattached on the cylinder. This separation existed on the cone for angles of attack up to 10°.

5. The pressures on the afterbody were found to be less than 4 percent of the pressure on the capsule face except for a few points on the canister at the 45° and 90° st[redacted]

[redacted]

6. The static stability tests show that for the escape, exit, and reentry versions, positive stability characteristics are indicated with the exit version having the lowest degree of stability. The escape and exit versions were indicated to have neutral stability at an angle of attack of about 8.5°, after which pitch-up tendencies occurred as angle of attack was increased.

Langley Research Center,
National Aeronautics and Space Administration,
Langley Field, Va., December 1, 1960.

I
1
2
2
0

[redacted]

REFERENCES

1. Bond, A. C., and Kehlet, A. B.: Review, Scope and Recent Results of Project Mercury Research and Development Program. Paper No. 60-35, Inst. Aero. Sci., Jan. 1960.

2. Pritts, O. R., and Mallard, S. R.: Pressure and Heat Transfer Distribution on a One-Tenth Scale Mercury Capsule at Mach Number 8. AEDC-TN-59-164 (Contract AF40(600)-800), Arnold Eng. Dev. Center, Jan. 1960.

3. Wallace, A. R., and Swain, W. N.: Static Stability, Heat Transfer, and Pressure Distribution Tests of NASA-McDonnell Mercury Models at Mach Numbers from 17 to 21. AEDC-TN-59-157, (Contract No. AF 40(600)-800), Arnold Eng. Dev. Center, Jan. 1960.

4. Shaw, David S., and Turner, Kenneth L.: Wind-Tunnel Investigation of Static Aerodynamic Characteristics of a 1/9-Scale Model of a Project Mercury Capsule at Mach Numbers from 1.60 to 4.65. NASA TM X-291, 1960.

5. Pearson, Albin O.: Wind-Tunnel Investigation at Mach Numbers from 0.50 to 1.14 of the Static Aerodynamic Characteristics of a Model of a Project Mercury Capsule. NASA TM X-292, 1960.

6. McLellan, Charles H., Williams, Thomas W., and Bertram, Mitchel H.: Investigation of a Two-Step Nozzle in the Langley 11-Inch Hypersonic Tunnel. NACA TN 2171, 1950.

7. Bertram, Mitchel H.: Boundary-Layer Displacement Effects in Air at Mach Numbers of 6.8 and 9.6. NASA TR R-22, 1959. (Supersedes NACA TN 4133.)

8. Crawford, Davis H.: Investigation of the Flow Over a Spiked-Nose Hemisphere-Cylinder at a Mach Number of 6.8. NASA TN D-118, 1959.

9. Chapman, Dean R.: A Theoretical Analysis of Heat Transfer in Regions of Separated Flow. NACA TN 3792, 1956.

10. Liepmann, H. W., and Roshko, A.: Elements of Gasdynamics. John Wiley & Sons, Inc., c1957, p. 105.

11. Kemp, N. H., and Riddell, F. R.: Heat Transfer to Satellite Vehicles Re-entering the Atmosphere. Res. Rep. 2, AVCO Res. Lab., Oct. 1956. (Formerly Res. Note 21.)

L 1220

[redacted]

12. Stoney, William E., Jr.: Aerodynamic Heating of Blunt Shapes at Mach Numbers up to 14. NACA RM L58E05a, 1958.

13. Crawford, Davis H., and McCauley, William D.: Investigation of the Laminar Aerodynamic Heat-Transfer Characteristics of a Hemisphere-Cylinder in the Langley 11-Inch Hypersonic Tunnel at a Mach Number of 6.8. NACA Rep. 1323, 1957. (Supersedes NACA TN 3706.)

14. Bertram, Mitchel H., and Feller, William V.: A Simple Method for Determining Heat Transfer, Skin Friction, and Boundary-Layer Thickness for Hypersonic Laminar Boundary-Layer Flows in a Pressure Gradient. NASA MEMO 5-24-59L, 1959.

15. Shaw, David S., and Turner, Kenneth L.: Wind-Tunnel Investigation of Static Aerodynamic Characteristics of a 1/9-Scale Model of a Possible Reentry Capsule at Mach Numbers from 2.29 to 4.65. NASA TM X-233, 1959.

L
1
2
2
0

[redacted]

DECLASSIFIED

L-1220

TABLE I.- RESULTS OF TESTS ON MERCURY CAPSULE, REENTRY CONFIGURATION

(a) $\alpha = 0^{\circ}$.

ϕ, deg	s/d	t_w, $^{\circ}F$	t_{aw}, $^{\circ}F$	q, $\frac{Btu}{ft^2\text{-}sec}$	h, $\frac{Btu}{ft^2\text{-}sec\text{-}^{\circ}R}$	N_{St}	R_s	p/p_t
0	0	132.8	1125	9.510	.009585	.013000	0	—
0	0.464	126.6	1125	8.417	.008430	.011500	1.170×10^5	2.5100×10^{-3}
0	0.666	93.5	967	0.438	.000507	.000690	1.681	0.0365
0	0.957	88.1	967	.162	.000185	.000259	2.413	.0627
0	1.248	90.7	967	.227	.000259	.000353	3.147	.0737
0	1.453	102.1	967	.451	.000522	.000711	3.664	—
0	1.605	99.6	967	.406	.000469	.000638	4.047	—
0	1.762	99.9	967	.576	.000665	.000905	4.444	—
0	1.914	113.7	967	.832	.000975	.001330	4.827	—
45	0.464	127.0	1125	8.484	.008501	.011600	1.170	2.4900
45	0.666	92.7	967	.462	.000528	.000719	1.681	.0441
45	0.957	87.8	967	.161	.000183	.000249	2.413	.0637
45	1.248	89.4	967	.218	.000249	.000339	3.147	.0734
45	1.453	100.4	967	.419	.000484	.000659	3.664	.0742
45	1.605	99.7	967	.416	.000479	.000653	4.047	.0911
45	1.762	99.4	967	.556	.000641	.000873	4.444	—
90	0.464	126.0	1125	7.903	.007911	.010800	1.170	2.5700
90	0.666	93.2	967	.466	.000534	.000727	1.681	.0409
90	0.957	87.4	967	.145	.000165	.000225	2.413	.0725
90	1.248	89.9	967	.213	.000243	.000330	3.147	.0753
90	1.453	99.1	967	.390	.000450	.000612	3.664	.0829
90	1.605	98.4	967	.375	.000432	.000588	4.047	.0975

(b) $\alpha = 0^{\circ}$. (Repeat run)

ϕ, deg	s/d	t_w, $^{\circ}F$	t_{aw}, $^{\circ}F$	q, $\frac{Btu}{ft^2\text{-}sec}$	h, $\frac{Btu}{ft^2\text{-}sec\text{-}^{\circ}R}$	N_{St}	R_s	p/p_t
0	0	163.3	1210	9.374	.008972	.013190	0	—
0	0.464	157.5	1210	8.588	.008163	.012000	1.036×10^5	—
0	0.666	107.0	1043	0.602	.000644	.000946	1.218	—
0	0.957	94.0	1043	.187	.000197	.000290	1.900	—
0	1.248	98.3	1043	.232	.000246	.000361	2.580	—
0	1.453	112.9	1043	.394	.000423	.000622	3.056	—
0	1.605	85.9	1043	.393	.000410	.000603	3.409	—
0	1.762	113.8	1043	.587	.000632	.000930	3.701	—
0	1.914	132.7	1043	.736	.000808	.001188	4.031	—
45	0.464	156.4	1210	8.270	.007846	.011540	1.036	—
45	0.666	107.5	1043	.614	.000657	.000966	1.218	—
45	0.957	93.6	1043	.192	.000202	.000297	1.900	—
45	1.248	97.4	1043	.241	.000255	.000375	2.580	—
45	1.453	112.0	1043	.391	.000420	.000618	3.056	—
45	1.605	111.1	1043	.417	.000448	.000658	3.409	—
45	1.762	113.1	1043	.589	.000634	.000932	3.701	—
90	0.464	155.7	1210	8.028	.007617	.011200	1.036	—
90	0.666	106.9	1043	.574	.000613	.000902	1.218	—
90	0.957	93.1	1043	.182	.000192	.000282	1.900	—
90	1.248	97.6	1043	.228	.000241	.000354	2.580	—
90	1.453	110.3	1043	.361	.000387	.000569	3.056	—
90	1.605	109.6	1043	.360	.000386	.000568	3.409	—

— No data available.

[redacted]

[redacted]

TABLE I.- RESULTS OF TESTS ON MERCURY CAPSULE, REENTRY CONFIGURATION - Continued

(c) $\alpha = 5^{\circ}$.

ϕ, deg	s/d	t_w, $^{\circ}F$	t_{aw}, $^{\circ}F$	q, $\frac{Btu}{ft^2\text{-}sec}$	h, $\frac{Btu}{ft^2\text{-}sec\text{-}^{\circ}R}$	N_{St}	R_s	p/p_t
0	0	161.6	1230	9.508	.008903	.013570	0	
0	0.464	161.8	1230	9.407	.008808	.013430	1.045×10^5	2.6800×10^{-3}
0	0.666	113.1	1061	0.704	.000743	.001133	1.501	0.0381
0	0.957	104.5	1061	0.337	.000352	.000536	2.155	0.0581
0	1.248	105.2	1061	0.376	.000393	.000600	2.810	0.0855
0	1.453	127.1	1061	0.607	.000650	.000990	3.272	—
0	1.605	120.4	1061	0.532	.000565	.000862	3.614	—
0	1.762	116.8	1061	0.649	.000687	.001048	3.968	—
0	1.914	129.9	1061	0.755	.000811	.001237	4.310	—
0	0	154.9	1190	10.140	.009797	.014370	0	—
0	-0.464	138.6	1190	7.995	.007607	.011150	1.081	2.3200
0	-0.666	95.8	1025	0.463	.000498	.000731	1.554	0.0618
0	-0.957	90.8	1025	.174	.000186	.000273	2.230	.0699
0	-1.248	94.4	1025	.221	.000238	.000350	2.909	.0740
0	-1.453	95.1	1025	.271	.000291	.000428	3.386	—
0	-1.605	92.8	1025	.267	.000287	.000420	3.740	—
0	-1.762	99.4	1025	.442	.000477	.000700	4.107	—
0	-1.914	110.6	1025	.603	.000660	.000968	4.461	—
45	0.464	147.3	1230	8.914	.008308	.012660	1.045	2.6300
45	0.666	110.7	1061	0.677	.000712	.001086	1.501	0.0341
45	0.957	101.3	1061	0.298	.000311	.000474	2.155	0.0579
45	1.248	103.4	1061	0.347	.000362	.000552	2.810	0.0742
45	1.453	125.2	1061	0.562	.000600	.000915	3.272	0.0955
45	1.605	121.1	1061	0.527	.000561	.000855	3.614	0.1390
45	1.762	115.6	1061	0.626	.000662	.001009	3.968	—
45	-0.464	139.1	1190	8.014	.007625	.011180	1.081	2.3300
45	-0.666	95.8	1025	.507	.000545	.000800	1.554	.0577
45	-0.957	86.7	1025	.130	.000138	.000203	2.230	.0670
45	-1.248	90.1	1025	.209	.000223	.000327	2.909	.0695
45	-1.453	98.2	1025	.314	.000339	.000497	3.386	.0725
45	-1.605	97.4	1025	.331	.000357	.000524	3.740	.0854
45	-1.762	101.4	1025	.487	.000527	.000773	4.107	—
90	0.464	153.2	1230	8.448	.007844	.011960	1.045	2.4500
90	0.666	106.1	1061	0.560	.000586	.000894	1.501	0.0374
90	0.957	94.6	1061	0.201	.000208	.000316	2.155	0.0631
90	1.248	99.1	1061	0.279	.000290	.000442	2.810	0.0684
90	1.453	115.4	1061	0.469	.000496	.000755	3.272	0.0770
90	1.605	11.5	1061	0.409	.000430	.000656	3.614	0.0902
90	-0.464	144.7	1190	8.659	.008286	.012150	1.081	2.500
90	-0.666	100.1	1025	.565	.000611	.000896	1.554	.0481
90	-0.957	89.5	1025	.193	.000206	.000303	2.230	.0672
90	-1.248	92.9	1025	.258	.000276	.000405	2.909	.0684
90	-1.453	104.1	1025	.371	.000403	.000590	3.386	.0742
90	-1.605	102.6	1025	.385	.000417	.000612	3.740	.0905

L-1220

[redacted]

DECLASSIFIED

2B

TABLE I.- RESULTS OF TESTS ON MERCURY CAPSULE, REENTRY CONFIGURATION - Continued

(d) $\alpha = 10^{\circ}$.

ϕ, deg	s/d	t_w, $^{\circ}F$	t_{aw}, $^{\circ}F$	q, $\frac{Btu}{ft^2\text{-}sec}$	h, $\frac{Btu}{ft^2\text{-}sec\text{-}^{\circ}R}$	N_{St}	R_s	P/P_t
0	0	156.6	1195	9.153	.008818	.012650	0	—
0	0.464	164.4	1195	9.800	.009505	.013640	1.109×10^5	2.8700×10^{-3}
0	0.666	124.6	1030	0.841	.000929	.001333	1.594	0.0534
0	0.957	121.4	1030	0.583	.000642	.000921	2.287	0.0783
0	1.248	121.2	1030	0.597	.000657	.000943	2.984	0.0977
0	1.453	142.3	1030	0.812	.000915	.001312	3.473	—
0	1.605	129.4	1030	0.635	.000705	.001011	3.837	—
0	1.762	120.3	1030	0.685	.000753	.001081	4.213	—
0	1.914	132.8	1030	0.749	.000835	.001197	4.576	—
0	0	149.8	1240	9.956	.009134	.014180	0	—
0	-0.464	134.3	1240	7.118	.006436	.009994	1.027	2.0600
0	-0.666	104.1	1070	0.347	.000357	.000554	1.476	0.0642
0	-0.957	102.7	1070	0.139	.000143	.000223	2.119	0.0689
0	-1.248	105.2	1070	0.160	.000166	.000258	2.764	0.0703
0	-1.453	109.4	1070	0.248	.000258	.000401	3.217	—
0	-1.605	108.0	1070	0.241	.000250	.000388	3.554	—
0	-1.762	114.0	1070	0.373	.000390	.000605	3.901	—
0	-1.914	121.1	1070	0.489	.000514	.000799	4.239	—
45	0.464	158.1	1195	9.305	.008973	.012870	1.109	—
45	0.666	117.0	1030	0.737	.000807	.001158	1.594	0.0399
45	0.957	115.5	1030	0.487	.000532	.000763	2.287	0.0613
45	1.248	116.7	1030	0.525	.000575	.000825	2.984	0.0839
45	1.453	133.6	1030	0.700	.000781	.001120	3.473	0.1300
45	1.605	126.2	1030	0.572	.000633	.000908	3.437	—
45	1.762	117.4	1030	0.638	.000699	.001003	4.213	—
45	-0.464	137.4	1240	7.382	.006693	.010390	1.027	2.1300
45	-0.666	104.9	1070	0.408	.000422	.000656	1.476	0.0607
45	-0.957	100.7	1070	0.125	.000129	.000201	2.119	0.0660
45	-1.248	104.1	1070	0.189	.000195	.000304	2.764	0.0674
45	-1.453	110.6	1070	0.291	.000304	.000472	3.217	0.0660
45	-1.605	110.9	1070	0.292	.000305	.000473	3.554	0.0727
45	-1.762	111.1	1070	0.404	.000421	.000654	3.901	—
90	0.464	148.9	1195	8.154	.007795	.011180	1.109	2.4000
90	0.666	108.5	1030	0.499	.000541	.000777	1.594	0.0311
90	0.957	101.7	1030	0.255	.000275	.000394	2.287	0.0547
90	1.248	101.7	1030	0.378	.000410	.000589	2.984	0.0685
90	1.453	122.6	1030	0.524	.000578	.000829	3.473	0.0867
90	1.605	115.2	1030	0.406	.000444	.000636	3.837	0.1020
90	-0.464	143.8	1240	8.280	.007555	.011730	1.027	2.4600
90	-0.666	109.3	1070	0.509	.000529	.000822	1.476	0.0499
90	-0.957	105.7	1070	0.259	.000269	.000417	2.119	0.0677
90	-1.248	109.4	1070	0.330	.000344	.000534	2.764	0.0710
90	-1.453	118.2	1070	0.435	.000457	.000710	3.217	0.0837
90	-1.605	116.2	1070	0.386	.000405	.000629	3.554	0.1044

L-1220

[redacted]

CONFIDENTIAL

TABLE I.- RESULTS OF TESTS ON MERCURY CAPSULE, REENTRY CONFIGURATION - Concluded

(e) $\alpha = 15^{\circ}$

ϕ, deg	s/d	t_w, $^{\circ}F$	t_{aw}, $^{\circ}F$	q, $\frac{Btu}{ft^2\text{-sec}}$	h, $\frac{Btu}{ft^2\text{-sec-}^{\circ}R}$	N_{St}	R_s	p/Pt
0	0	143.0	1190	9.197	.008784	.012620	0	—
0	0.464	137.9	1190	10.110	.009797	.014080	1.109×10^5	—
0	0.666	151.2	1025	1.064	.001188	.001707	1.594	—
0	0.957	157.5	1025	0.865	.000965	.001386	2.287	—
0	1.248	129.2	1025	0.817	.000907	.001304	2.984	—
0	1.453	128.6	1025	1.102	.001256	.001805	3.473	—
0	1.605	124.9	1025	0.763	.000851	.001223	3.837	—
0	1.762	147.9	1025	0.818	.000904	.001299	4.213	—
0	1.914	128.7	1025	0.906	.001017	.001461	4.576	—
45	0.464	119.6	1190	9.655	.009293	.013350	1.109	—
45	0.666	134.4	1025	0.865	.000953	.001369	1.594	—
45	0.957	117.4	1025	0.689	.000762	.001095	2.287	—
45	1.248	120.6	1025	0.708	.000782	.001123	2.984	—
45	1.453	119.2	1025	0.871	.000979	.001407	3.473	—
45	1.605	135.5	1025	0.669	.000742	.001066	3.837	—
45	1.762	123.3	1025	0.763	.000837	.001203	4.213	—
90	0.464	114.4	1190	7.654	.007276	.010450	1.109	—
90	0.666	102.6	1025	0.485	.000526	.000755	1.594	—
90	0.957	100.8	1025	0.349	.000378	.000543	2.287	—
90	1.248	107.4	1025	0.464	.000506	.000727	2.984	—
90	1.453	116.3	1025	0.586	.000644	.000926	3.473	—
90	1.605	107.2	1025	0.424	.000462	.000664	3.837	—

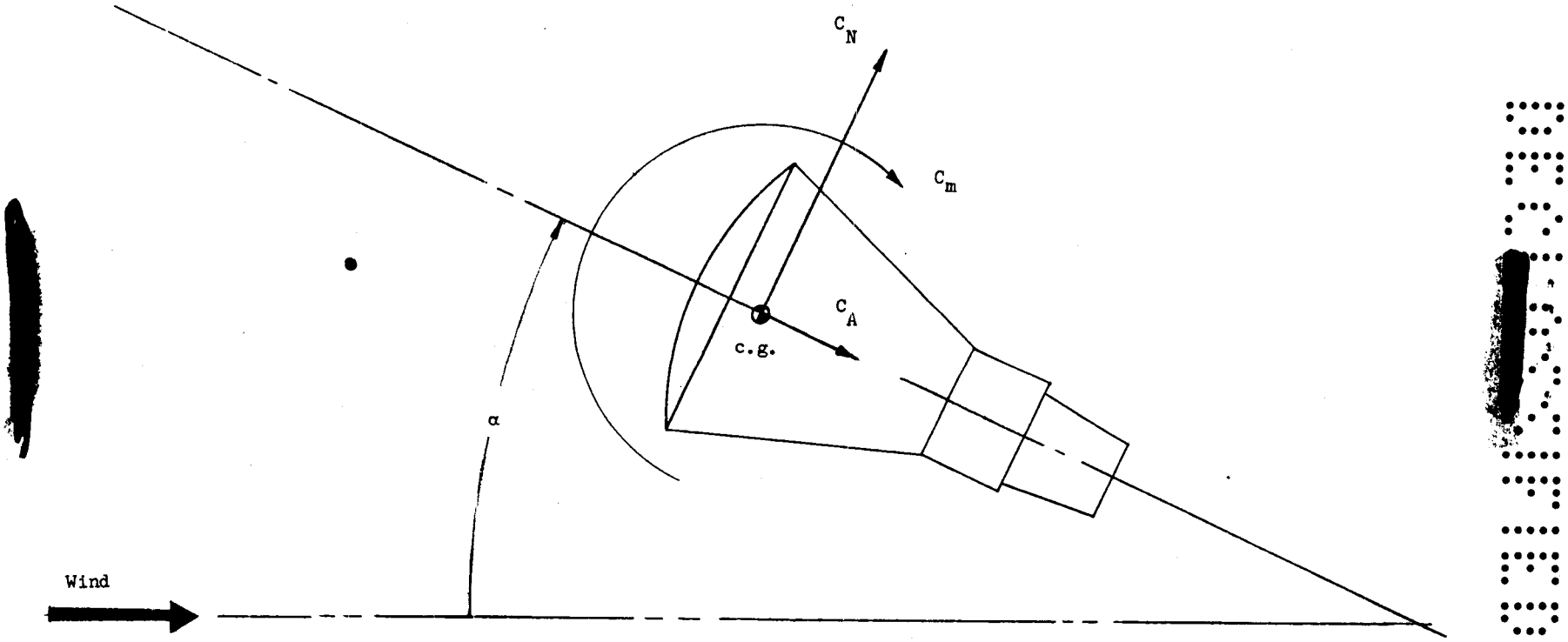

Figure 1.- Body-axis system (reentry version shown). Arrows indicate positive directions.

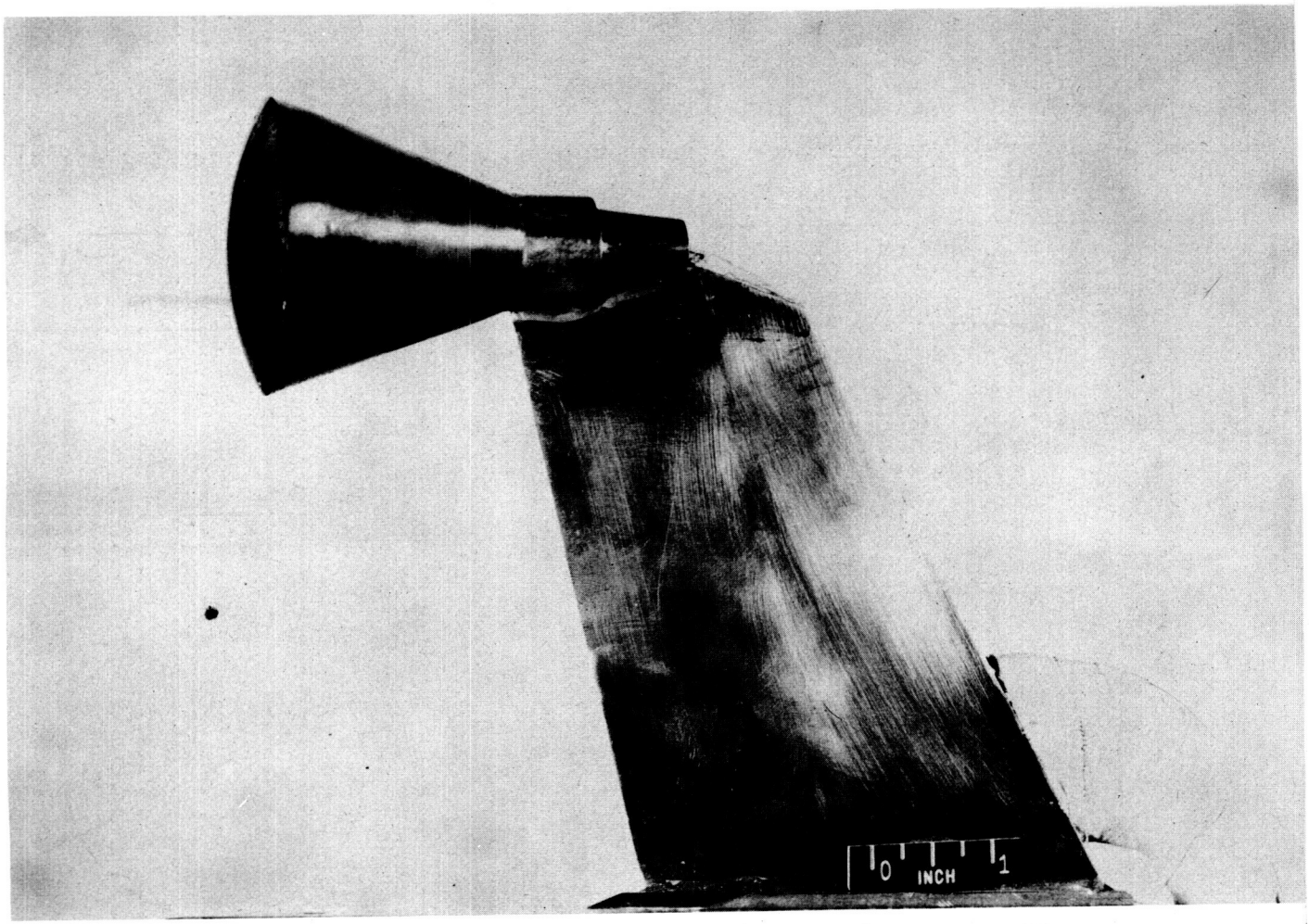

(a) View of model with floor mount. L-59-5734

Figure 2.- Heat-transfer and pressure-distribution model.

L-1220

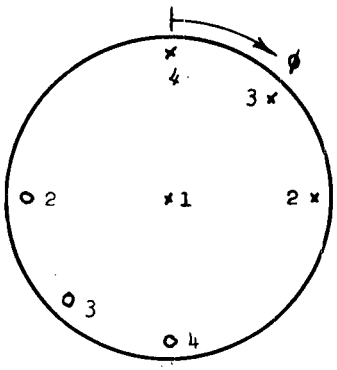

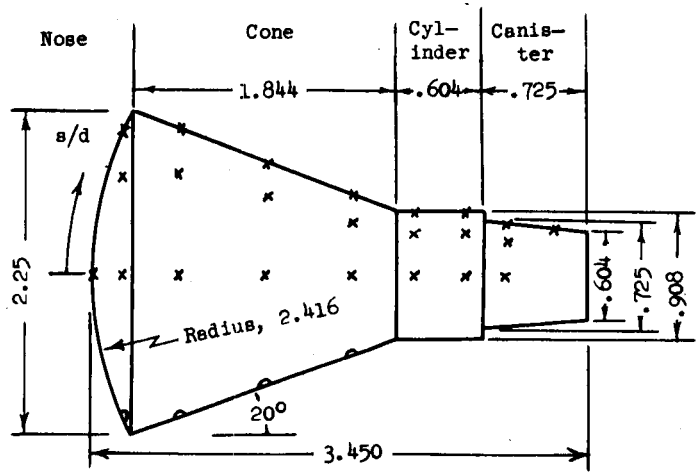

ORIFICE AND THERMOCOUPLE LOCATIONS			
Thermo-couple	Orifice	ϕ, deg	s/d
1	None	0	0
2	2	90	0.464
3	3	45	0.464
4	4	0	0.464
5	5	0	0.666
6	6	0	0.957
7	7	0	1.248
8	None	0	1.453
9	None	0	1.605
10	None	0	1.762
11	None	0	1.914
12	12	45	0.666

ORIFICE AND THERMOCOUPLE LOCATIONS			
Thermo-couple	Orifice	ϕ, deg	s/d
13	13	45	0.957
14	14	45	1.248
15	15	45	1.453
16	16	45	1.605
17	None	45	1.762
18	18	90	0.666
19	19	90	0.957
20	20	90	1.248
21	21	90	1.453
22	22	90	1.605
23	23	90	1.762

x Thermocouple
o Pressure orifice

(b) Model details with pressure-orifice and thermocouple locations. (All dimensions are in inches.)

Figure 2.- Concluded.

[redacted]

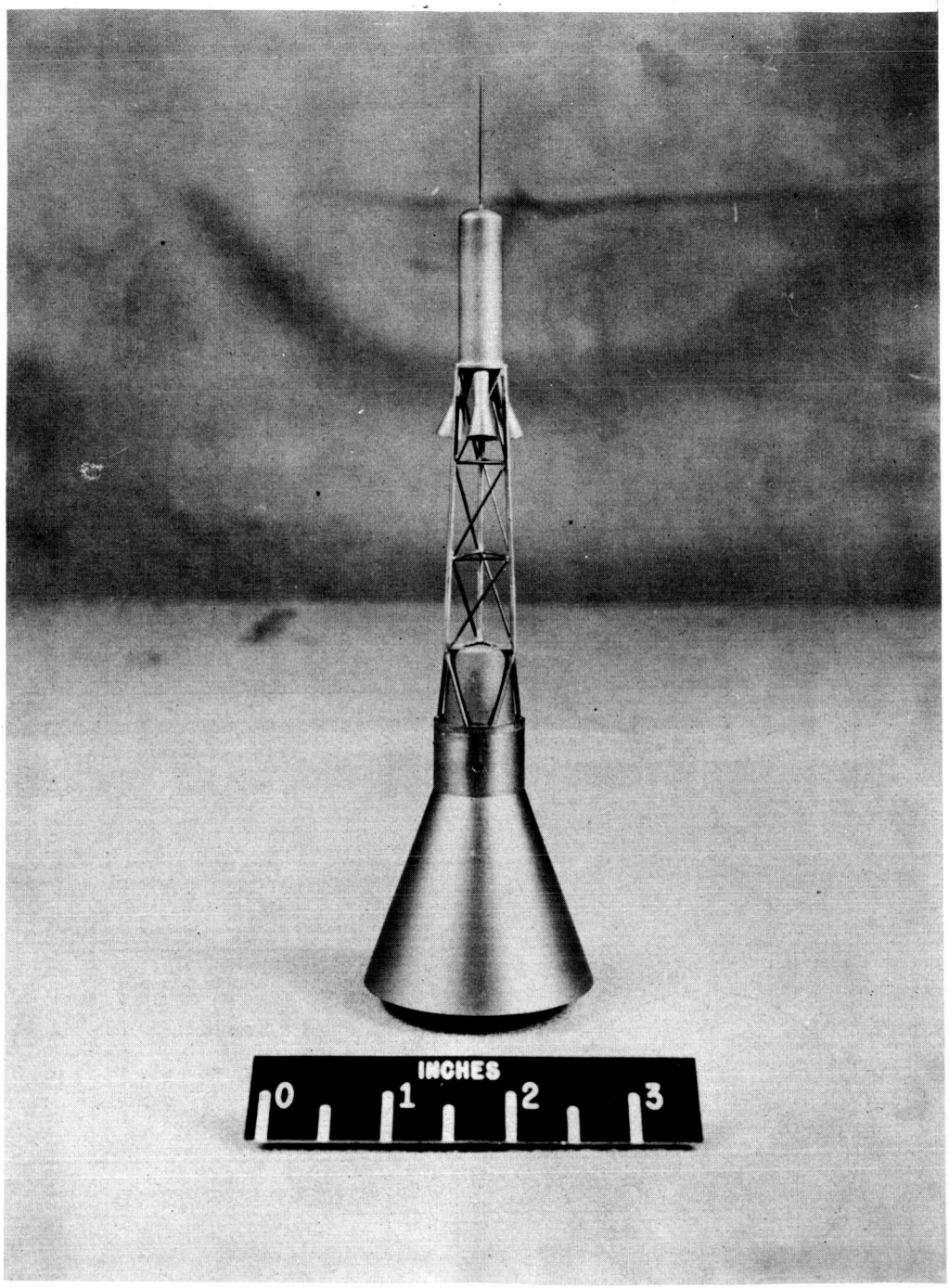

(a) Escape version. L-59-1717

Figure 3.- Mercury capsule force-test configurations.

L-1220

[redacted]

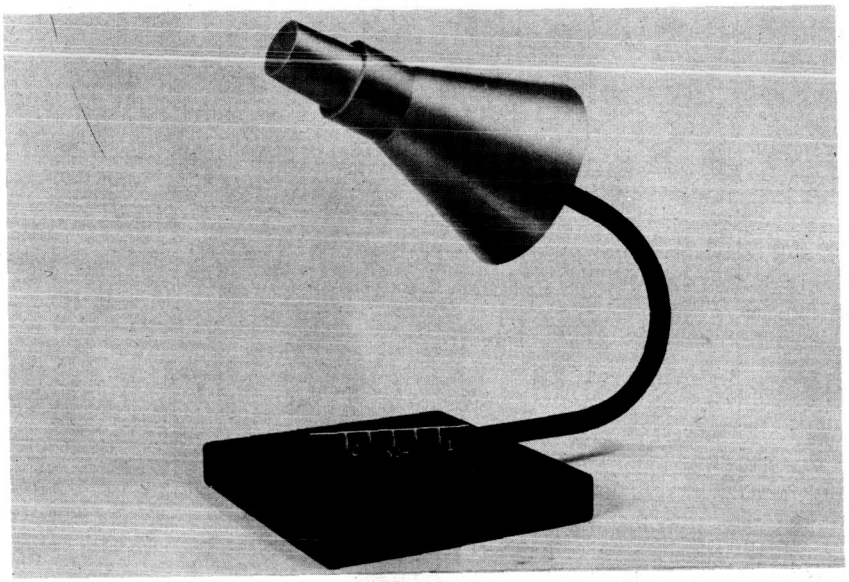

(b) Exit version.

(c) Reentry version. L-60-6958

Figure 3.- Continued.

L-1220

[redacted]

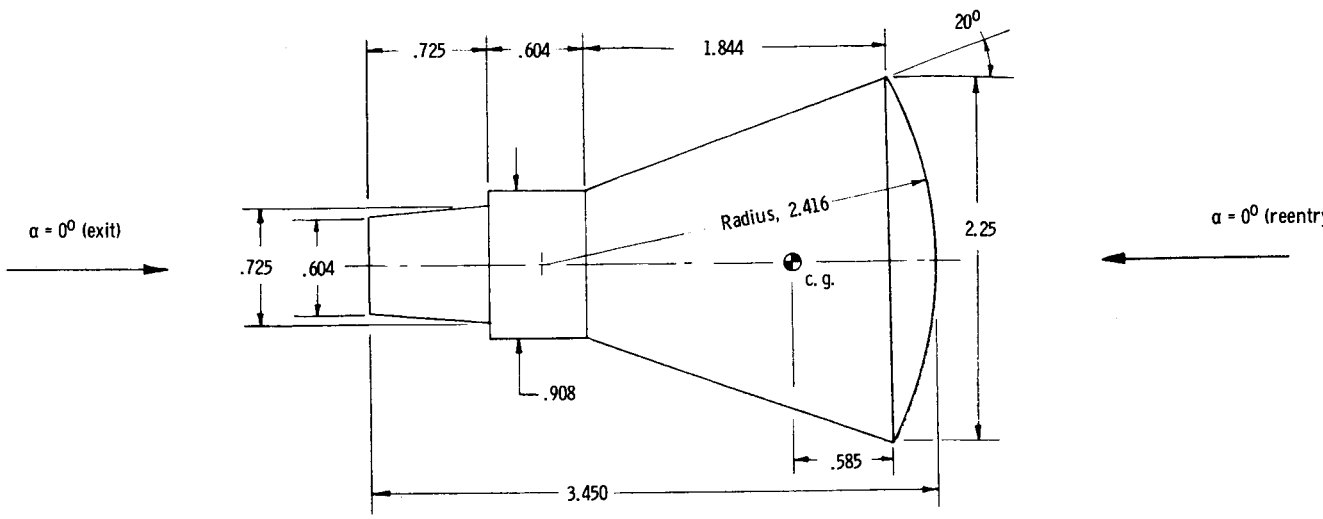

Exit-reentry versions

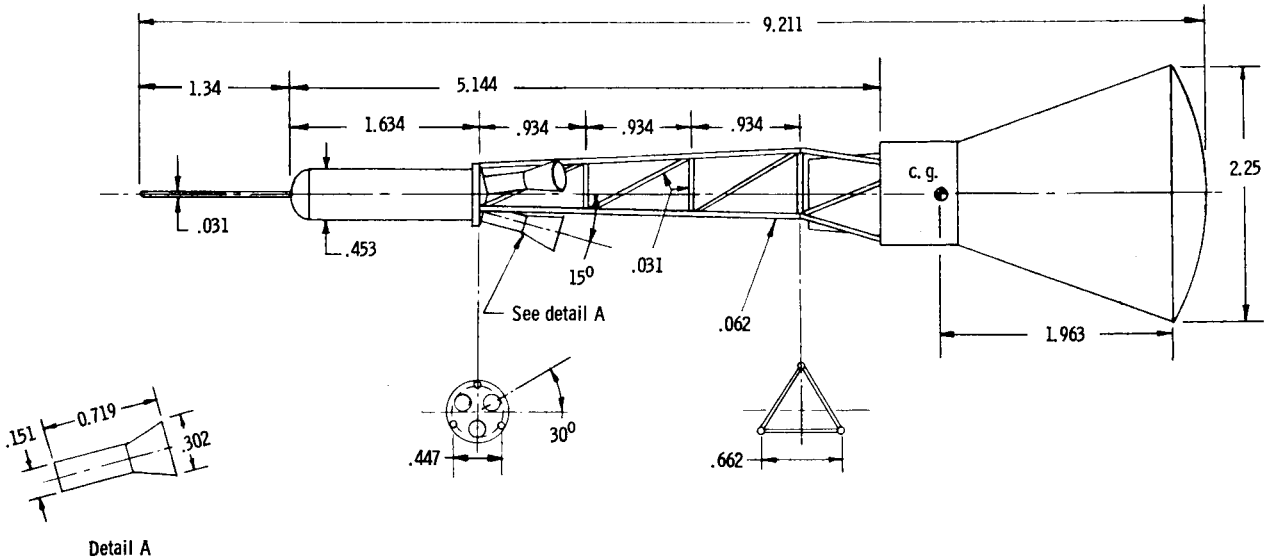

Detail A

Escape version

(d) Model detail.

Figure 3.- Concluded.

[redacted]

I-1220

DECLASSIFIED

L-1220

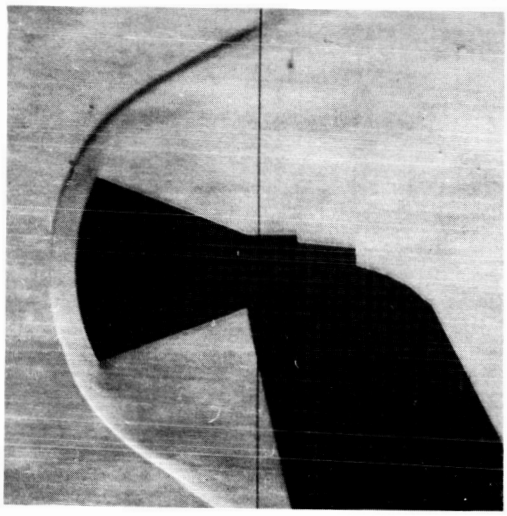

(a) $\alpha = 0°$.

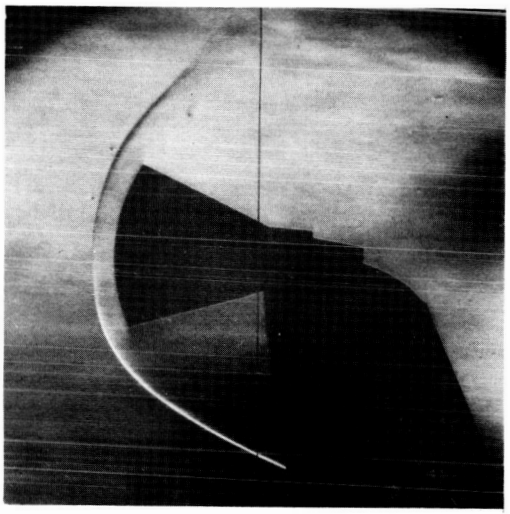

(b) $\alpha = 5°$.

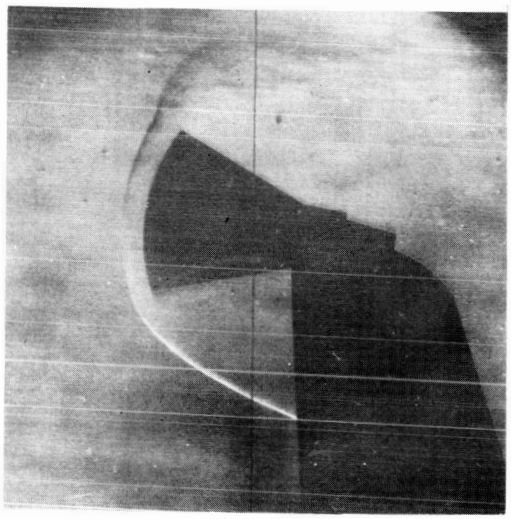

(c) $\alpha = 10°$.

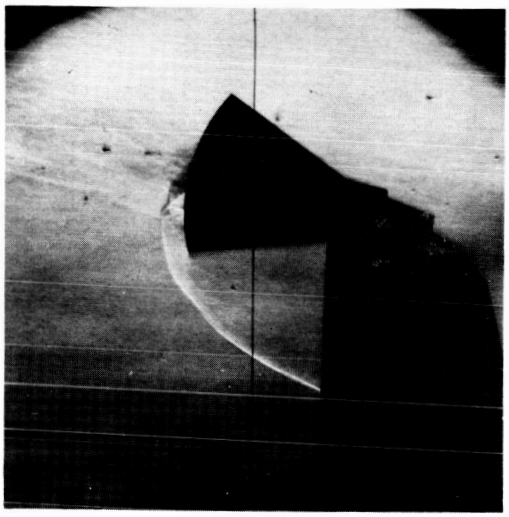

(d) $\alpha = 15°$.

L-60-6959

Figure 4.- Schlieren photographs of floor-mounted model at angle of attack. M = 9.6.

[redacted]

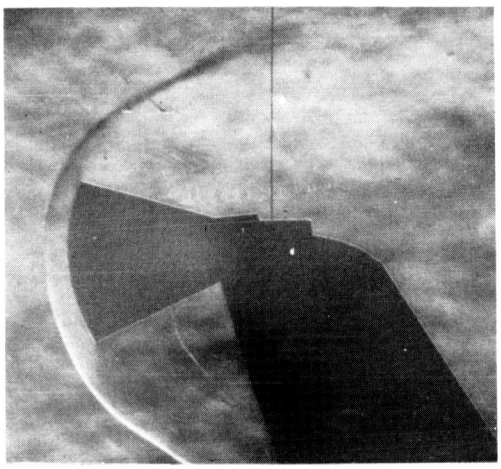

(e) $\alpha = -5°$.

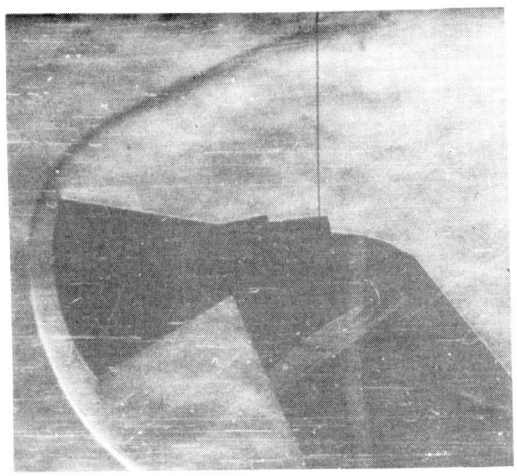

(f) $\alpha = -10°$.

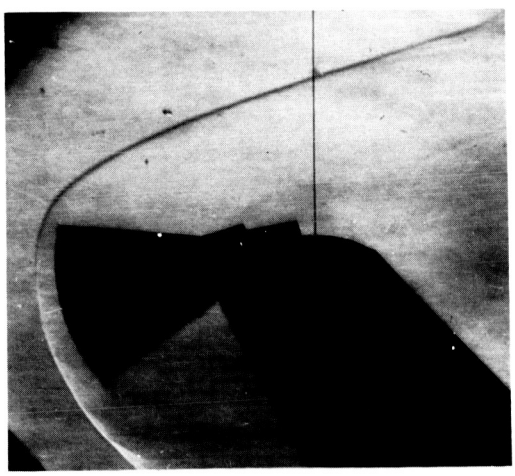

(g) $\alpha = -15°$.

Figure 4.- Concluded. L-60-6960

L-1220

[redacted]

L-1220

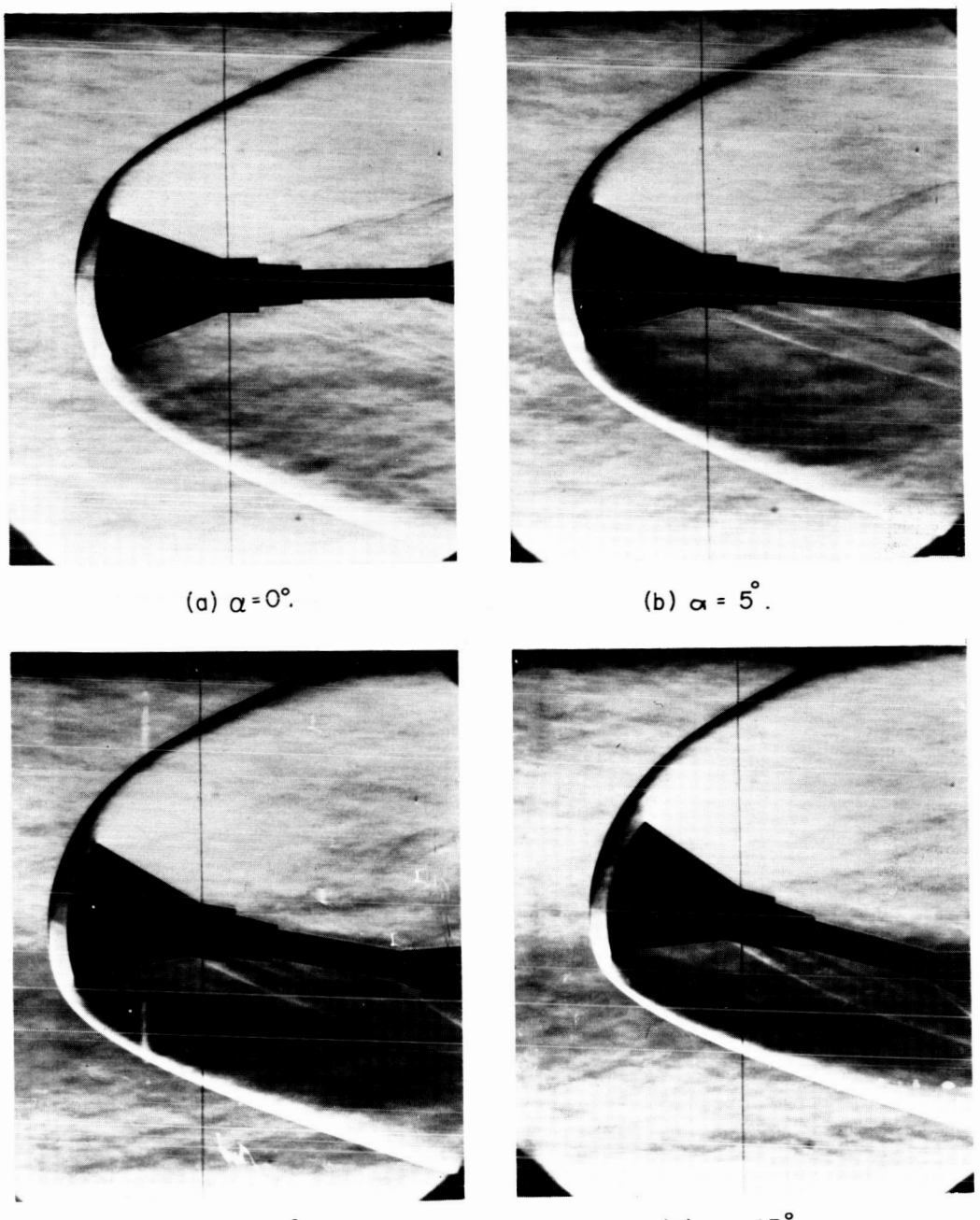

(a) $\alpha = 0°$.

(b) $\alpha = 5°$.

(c) $\alpha = 10°$.

(d) $\alpha = 15°$.

L-60-6961

Figure 5.- Schlieren flow studies of sting-mounted model at angle of attack. M = 6.9.

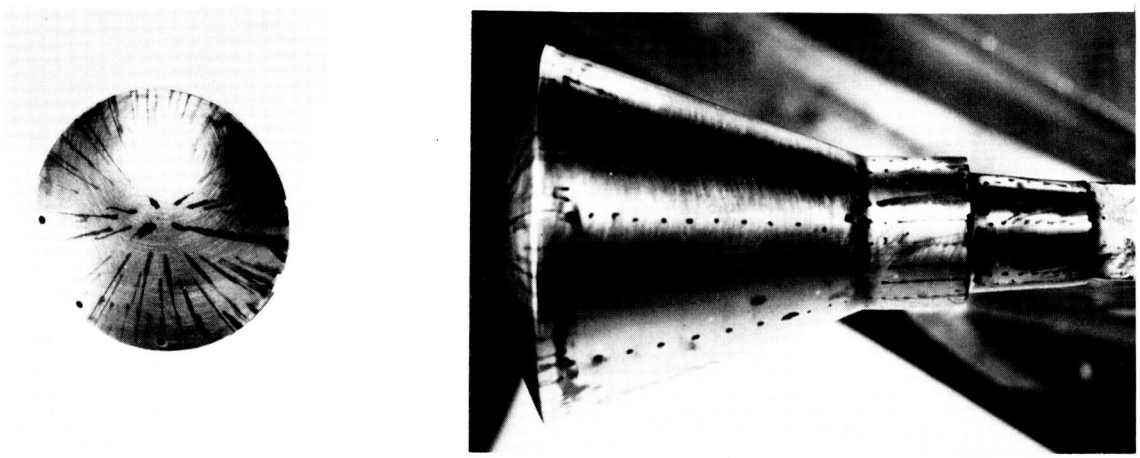

Front View

Top View

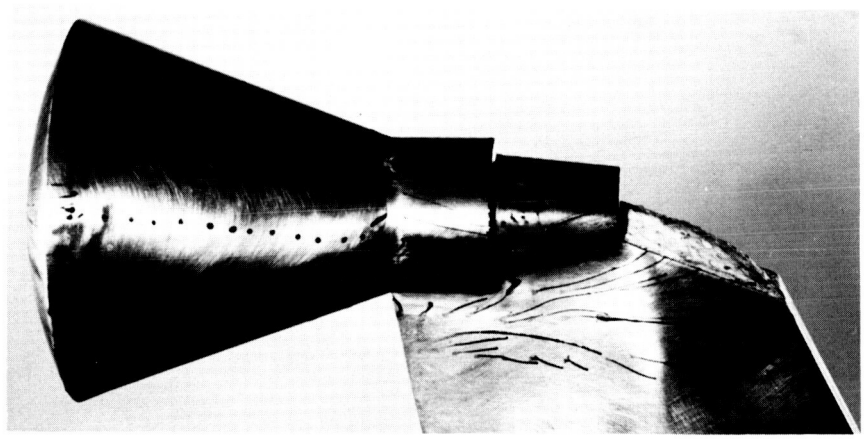

Air Flow

Side View

(a) $\alpha = 0^{\circ}$. L-60-6962

Figure 6.- Oil-flow study of floor-mounted model at angle of attack. M = 6.9.

L-1220

DECLASSIFIED

L-1220

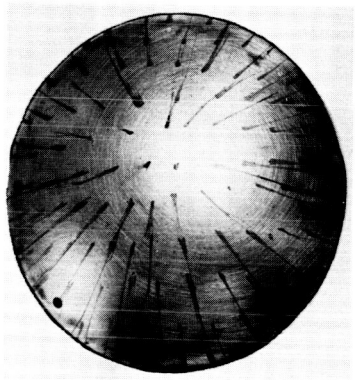

Front View

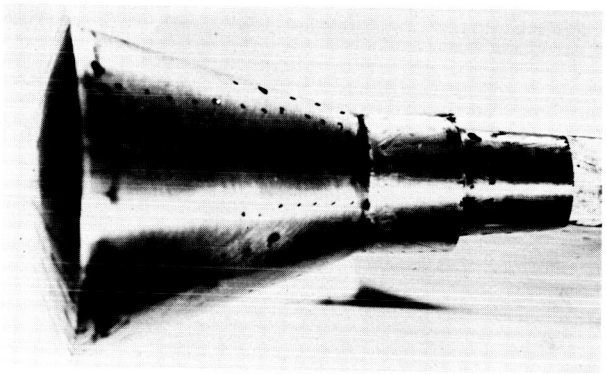

Top View

Air Flow

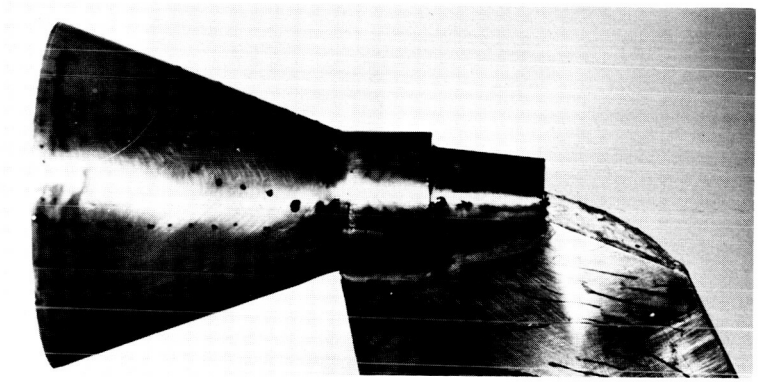

Side View

(b) $\alpha = 5^{\circ}$. L-60-6963

Figure 6.- Continued.

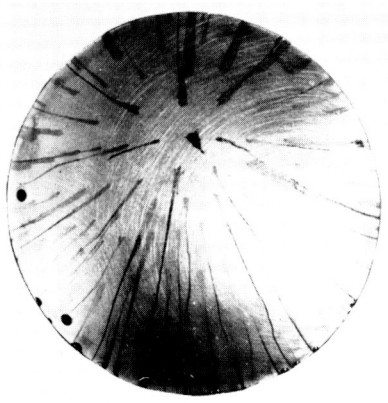

Front View

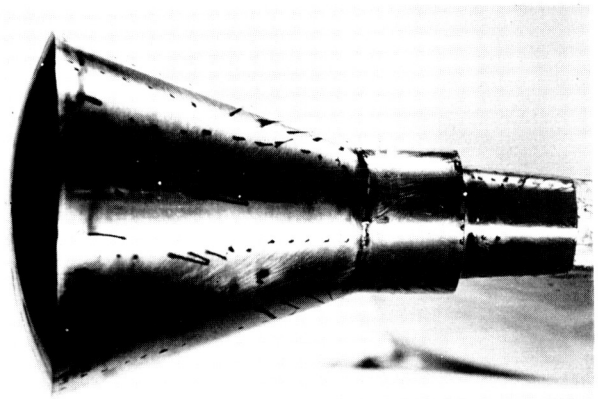

Top View

Air Flow

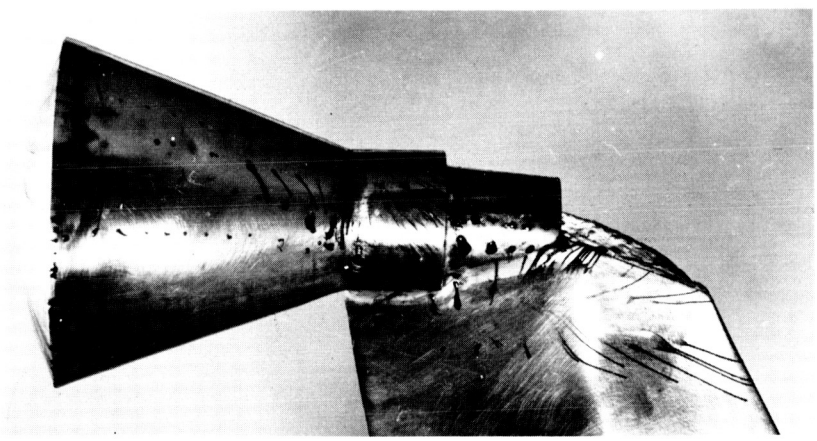

Side View

(c) $\alpha = 10^{\circ}$.

L-60-6964

Figure 6.- Continued.

L-1220

DECLASSIFIED

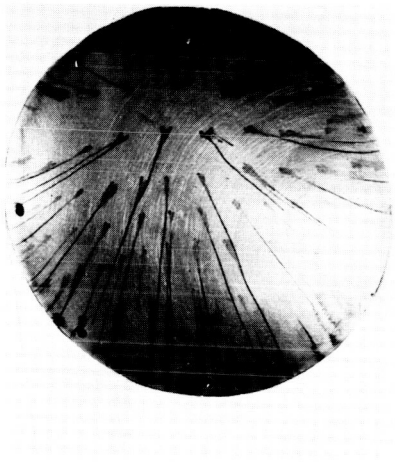

Front View

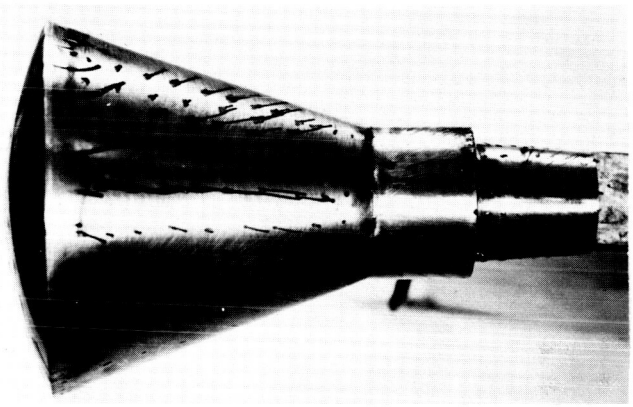

Top View

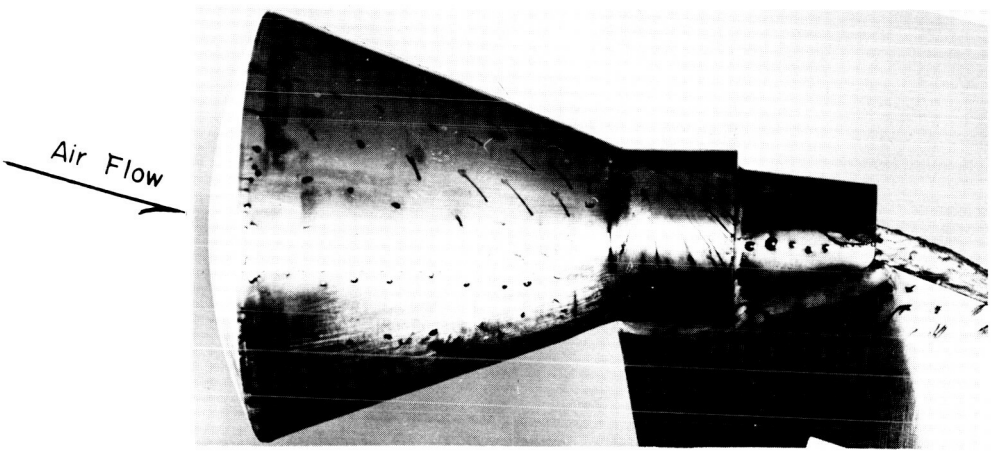

Side View

(d) $\alpha = 15^{\circ}$. L-60-6965

Figure 6.- Continued.

[redacted]

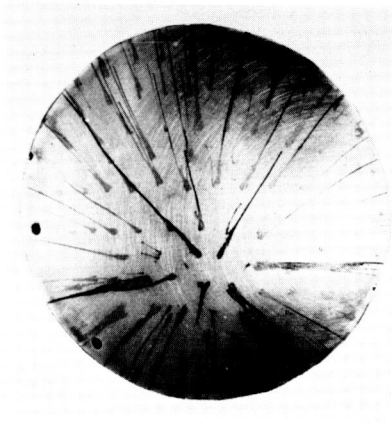

Front View

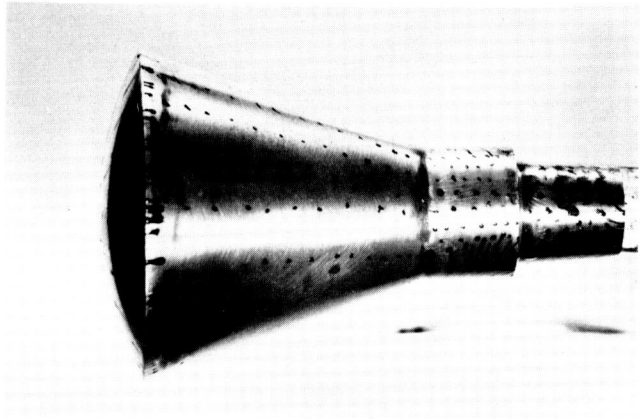

Top View

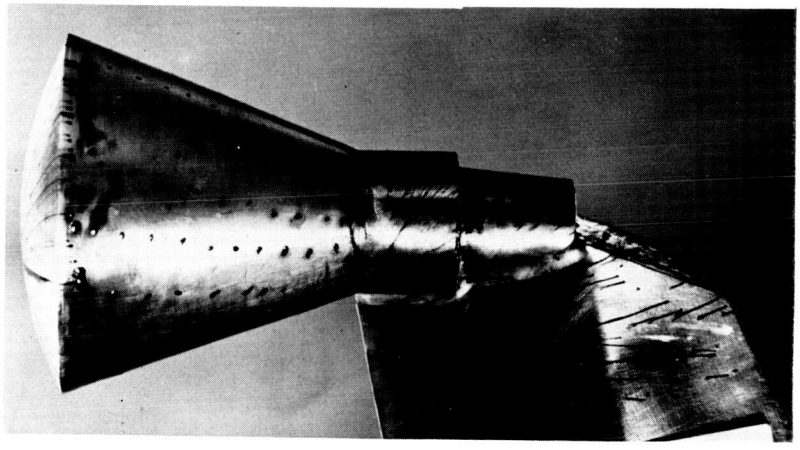

Side View

(e) $\alpha = -10^{\circ}$. L-60-6966

Figure 6.- Concluded.

L-1220

[redacted]

4B

DECLASSIFIED

L-1220

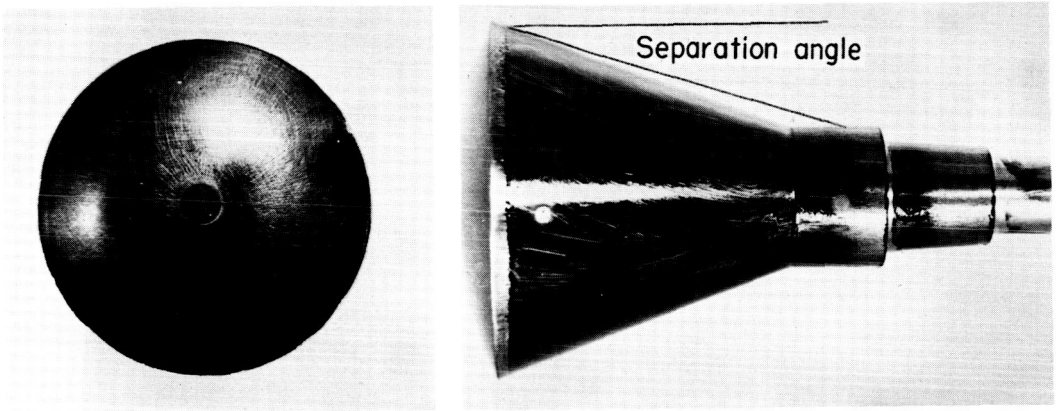

Front View Top View

(a) $\alpha = 0^{\circ}$.

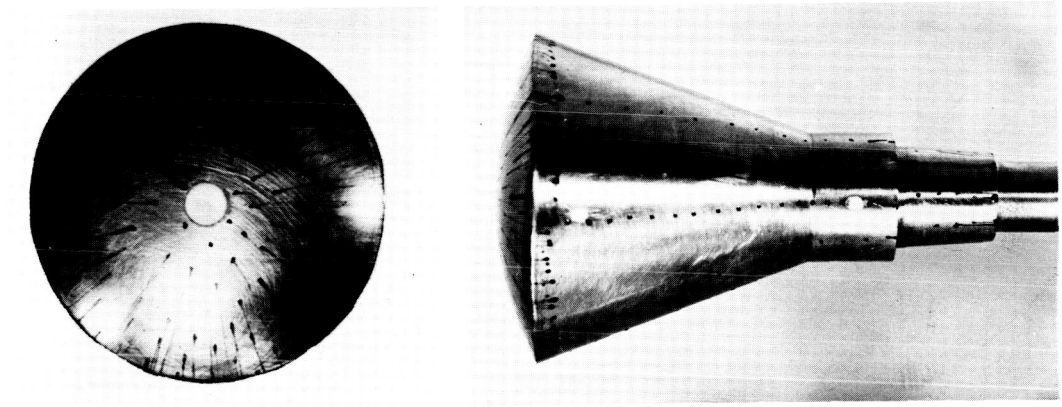

Front View Top View

(b) $\alpha = 0^{\circ}$. L-60-6967

Figure 7.- Oil-flow study of sting-mounted model at angle of attack. M = 6.9.

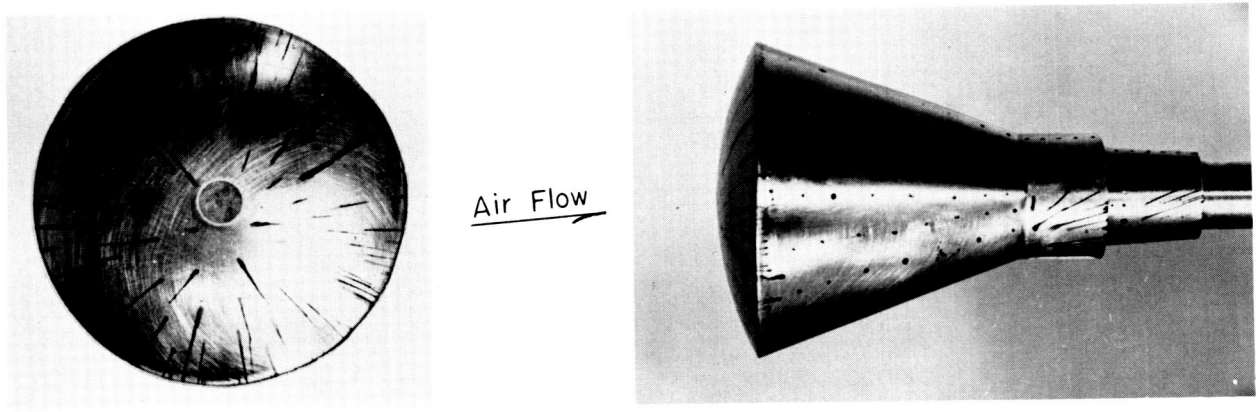

(c) $\alpha = 5^{\circ}$. L-60-6968

Figure 7.- Continued.

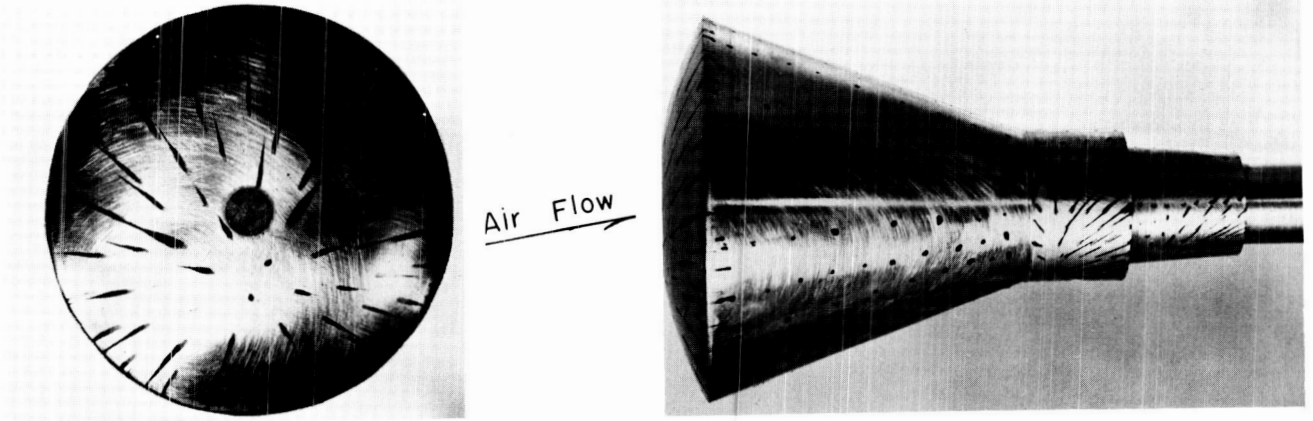

Front View

Side View

Bottom View

Top View

(d) $\alpha = 10^{\circ}$. L-60-6969

Figure 7.- Continued.

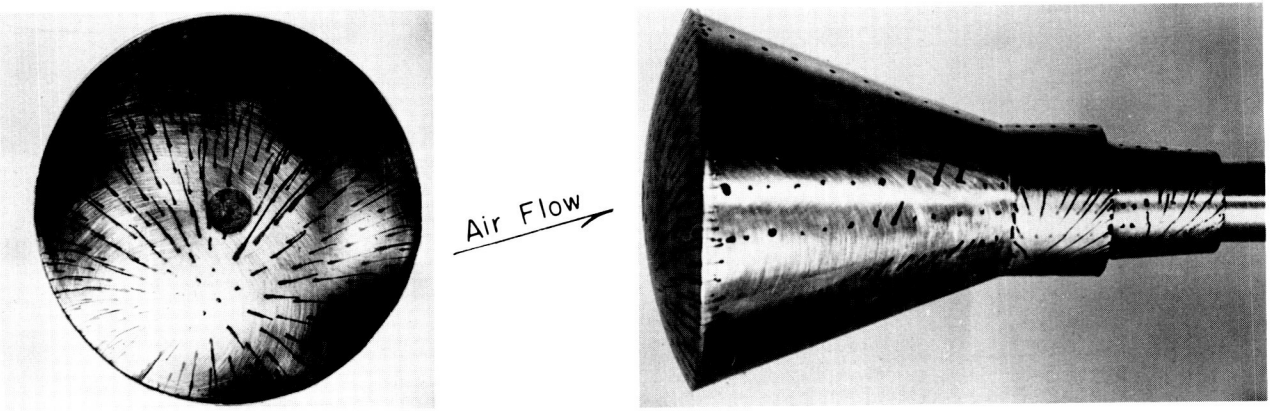

Front View

Side View

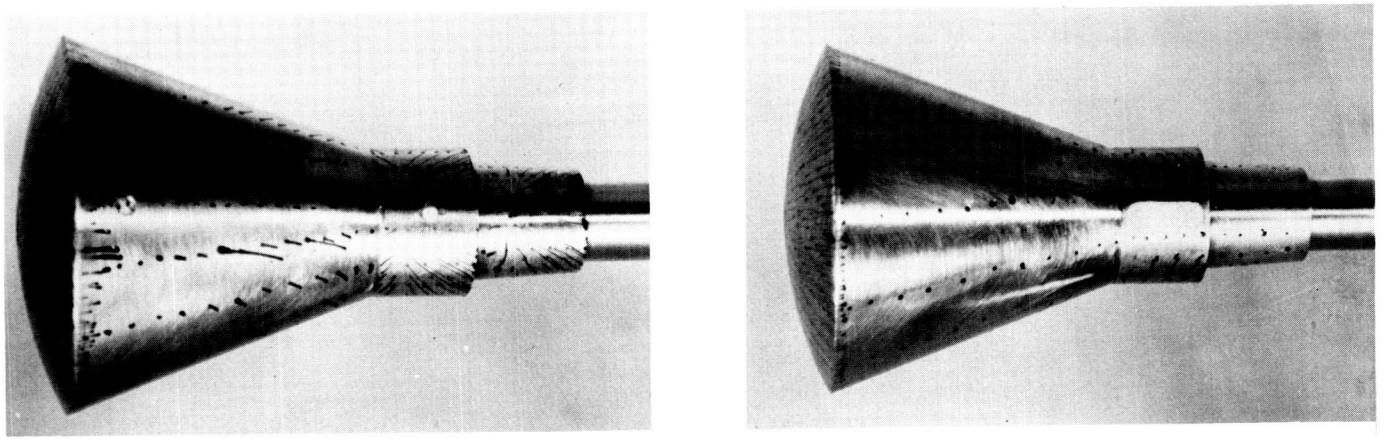

Bottom View

Top View

(e) $\alpha = 15^{\circ}$. L-60-6970

Figure 7.- Continued.

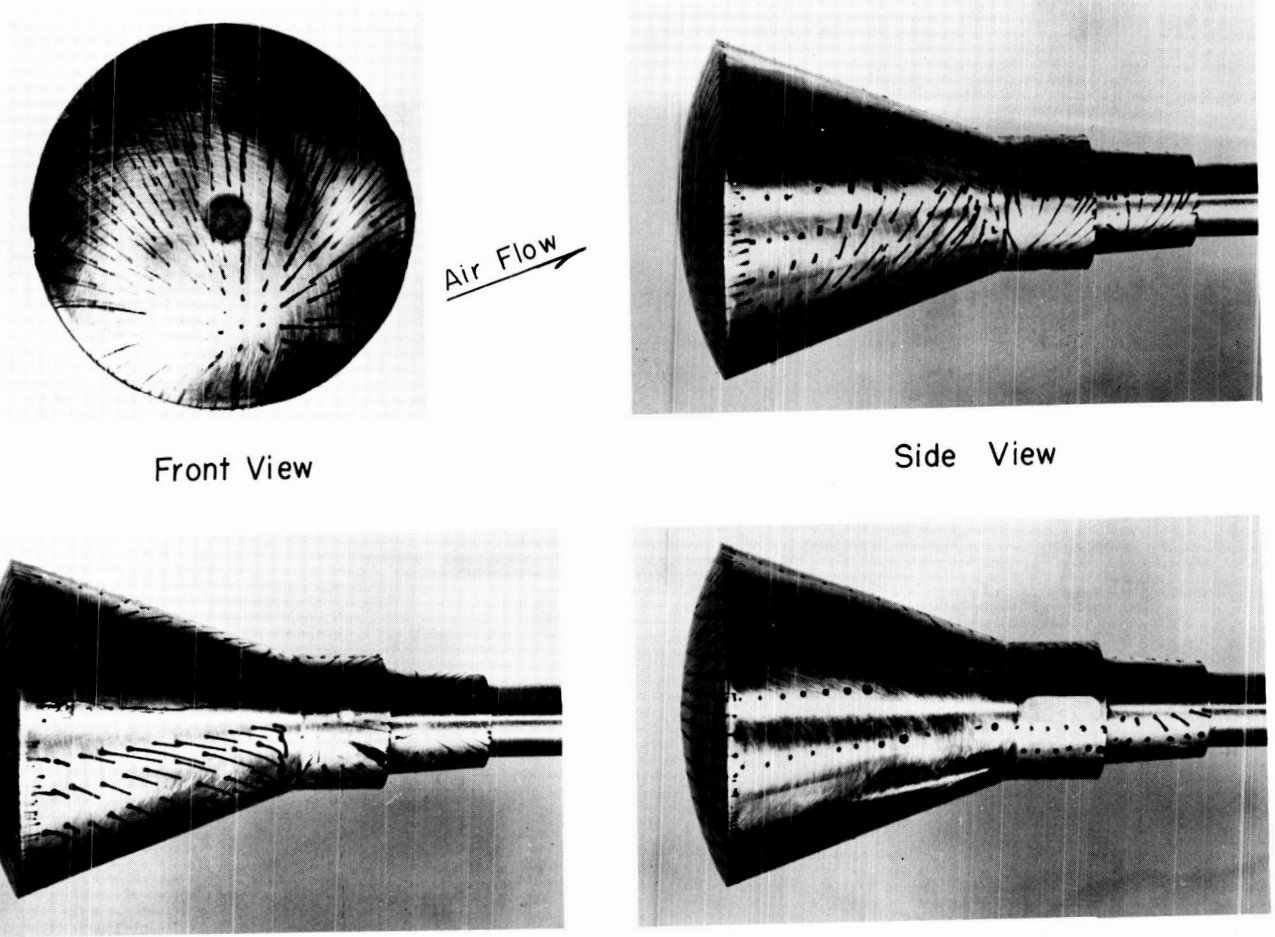

(f) $\alpha = 20^{\circ}$. L-60-6971

Figure 7.- Concluded.

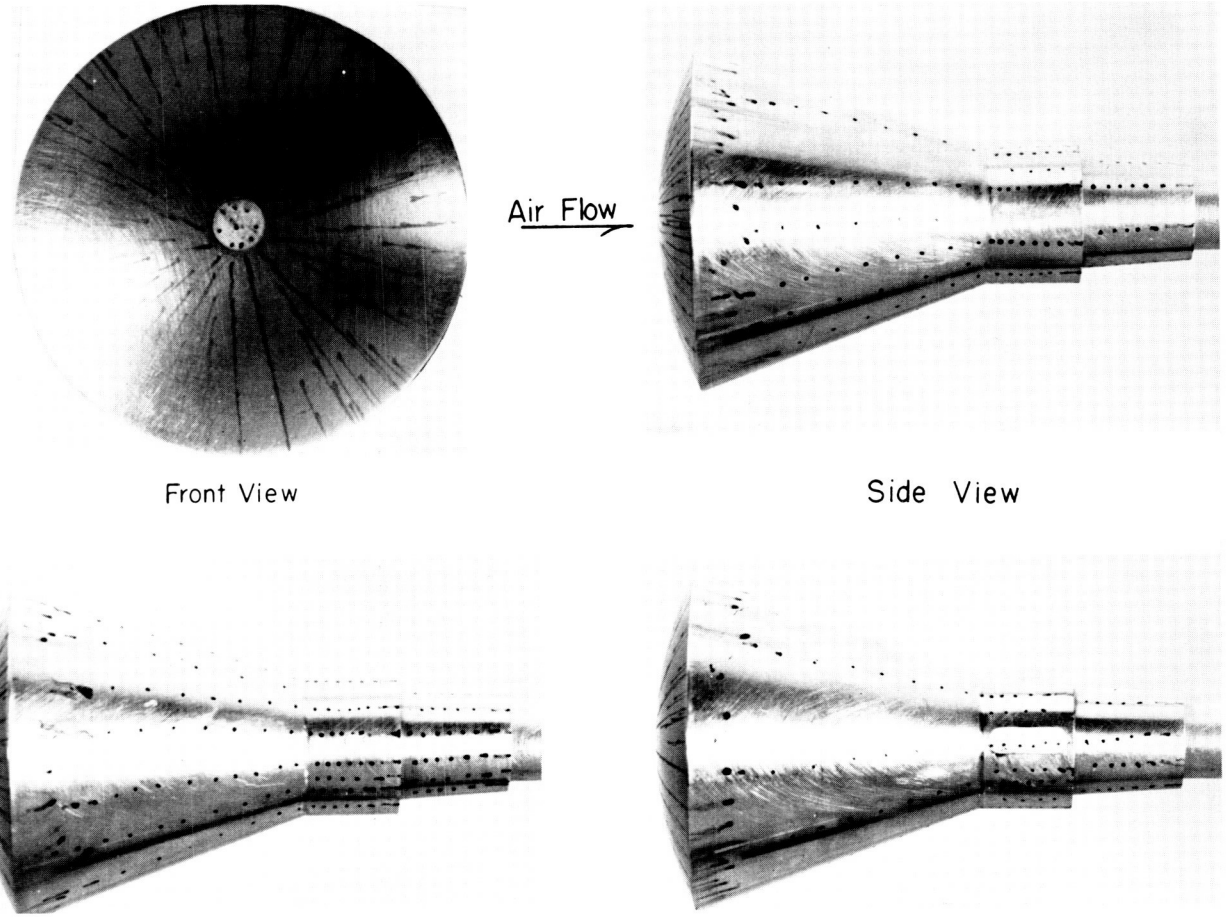

(a) $\alpha = 0^{\circ}$. L-60-6972

Figure 8.- Oil-flow study of sting-mounted model at angle of attack. M = 9.6.

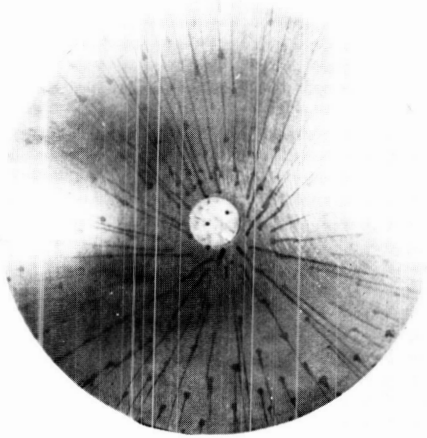

Front View

Air Flow

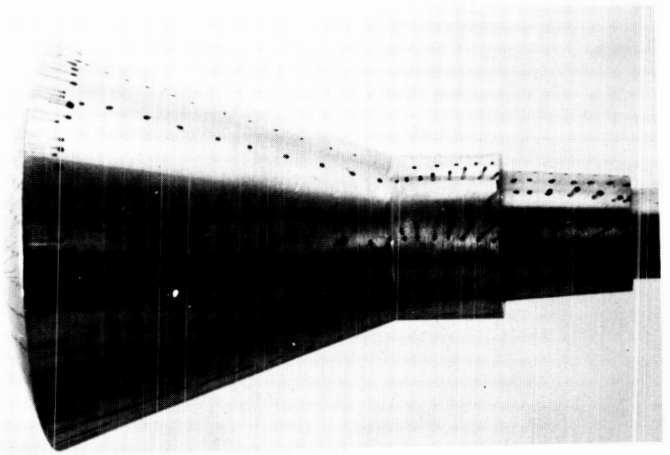

Side View

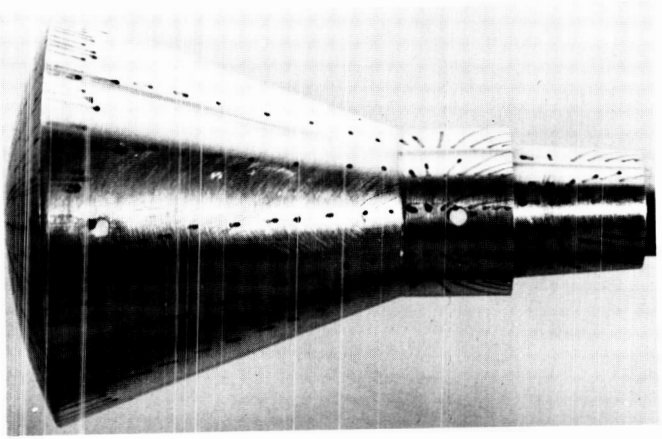

Bottom View

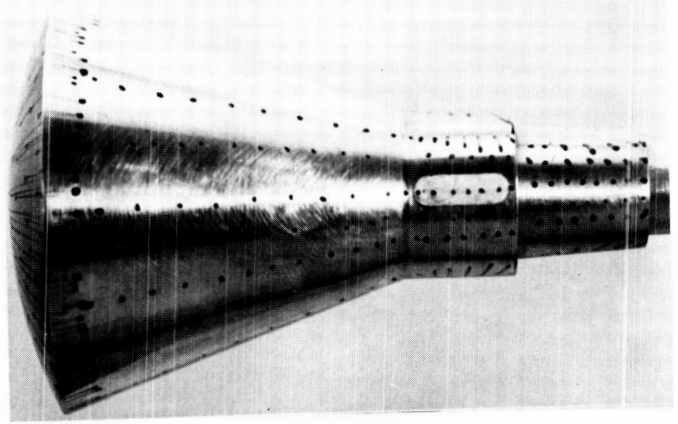

Top View

(b) $\alpha = 5^{\circ}$. L-60-6973

Figure 8.- Continued.

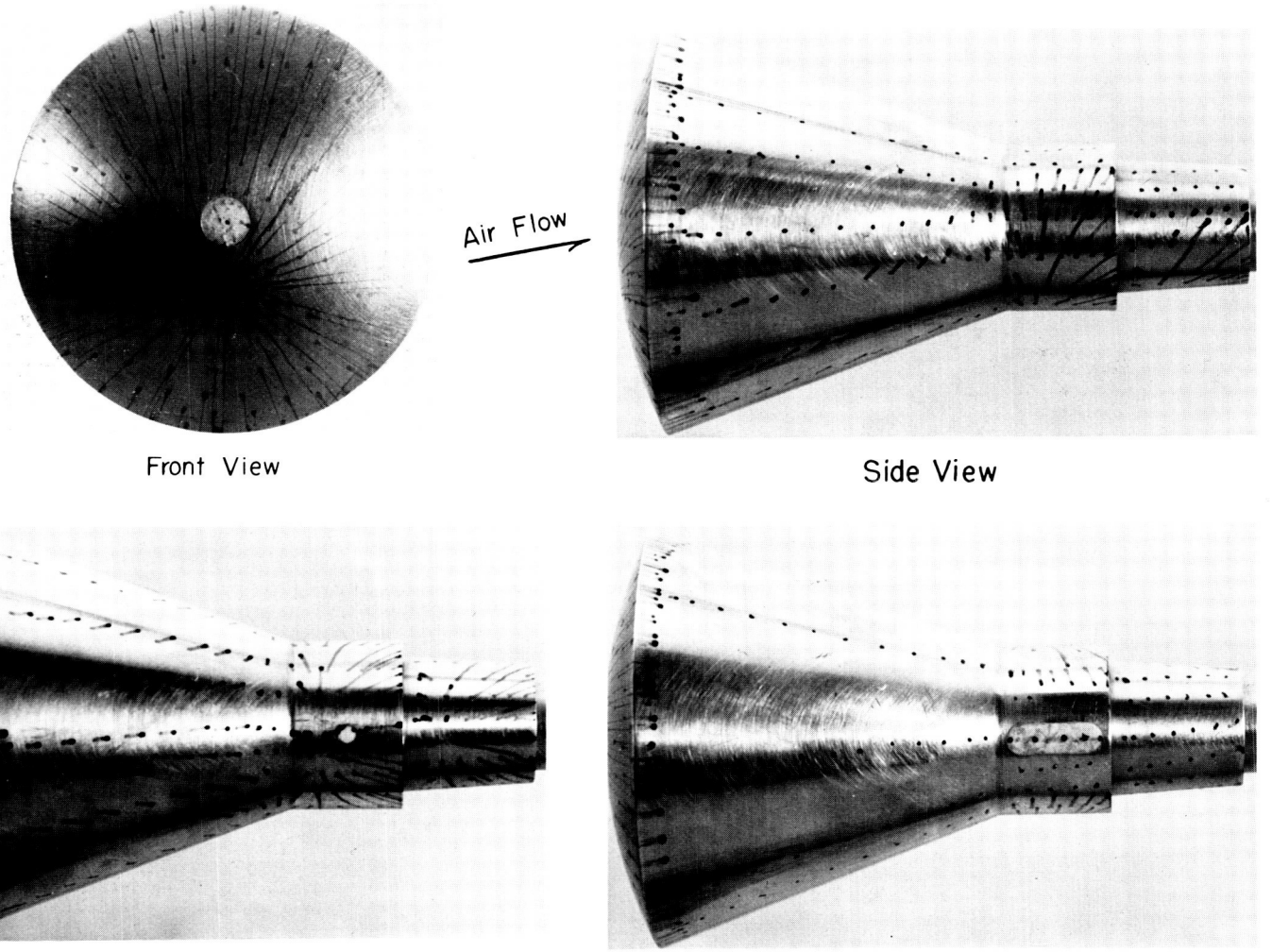

(c) $\alpha = 10^{\circ}$. L-60-6974

Figure 8.- Continued.

NASA-Langley, 1960 L-1220

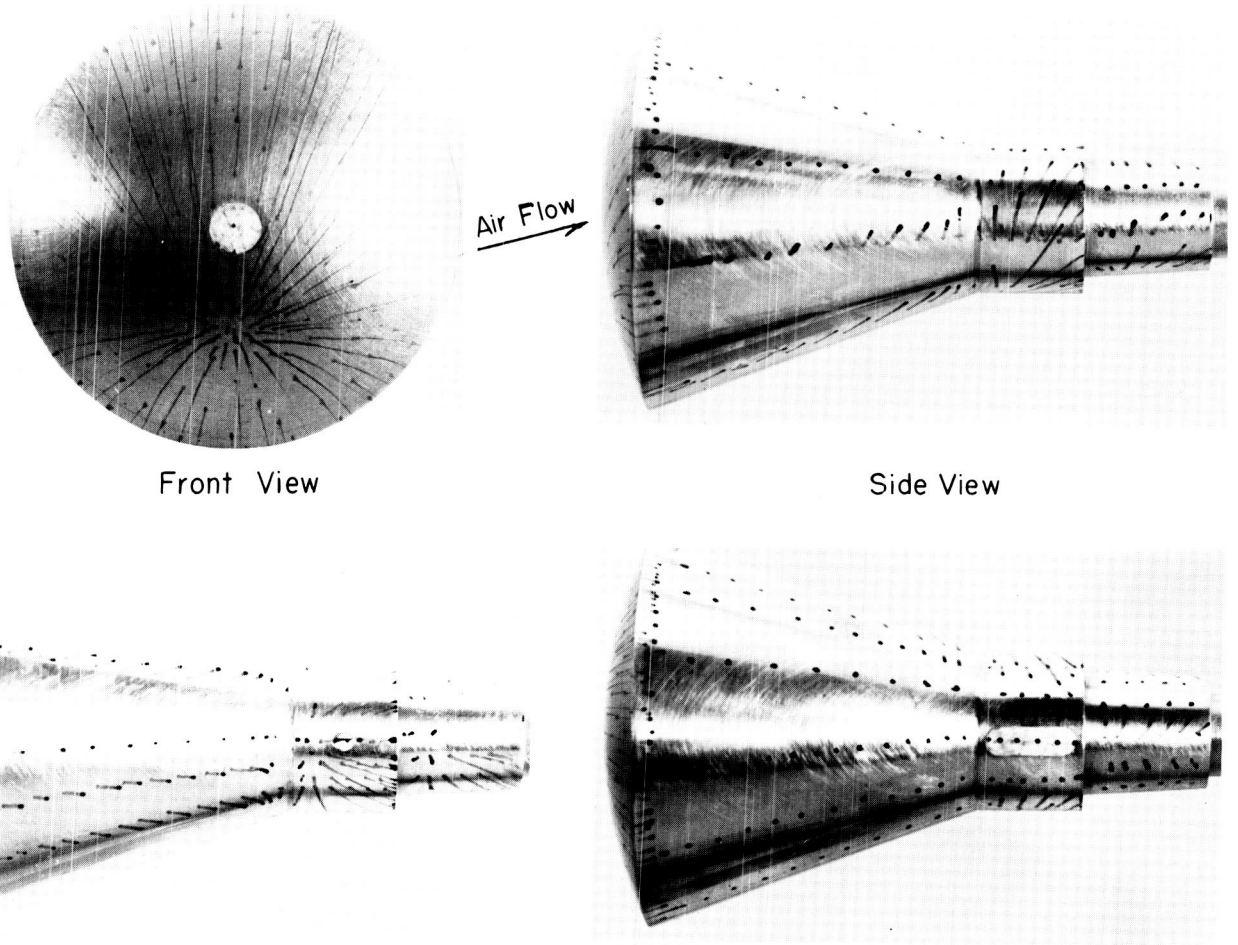

(d) $\alpha = 15^{\circ}$. L-60-6975

Figure 8.- Continued.

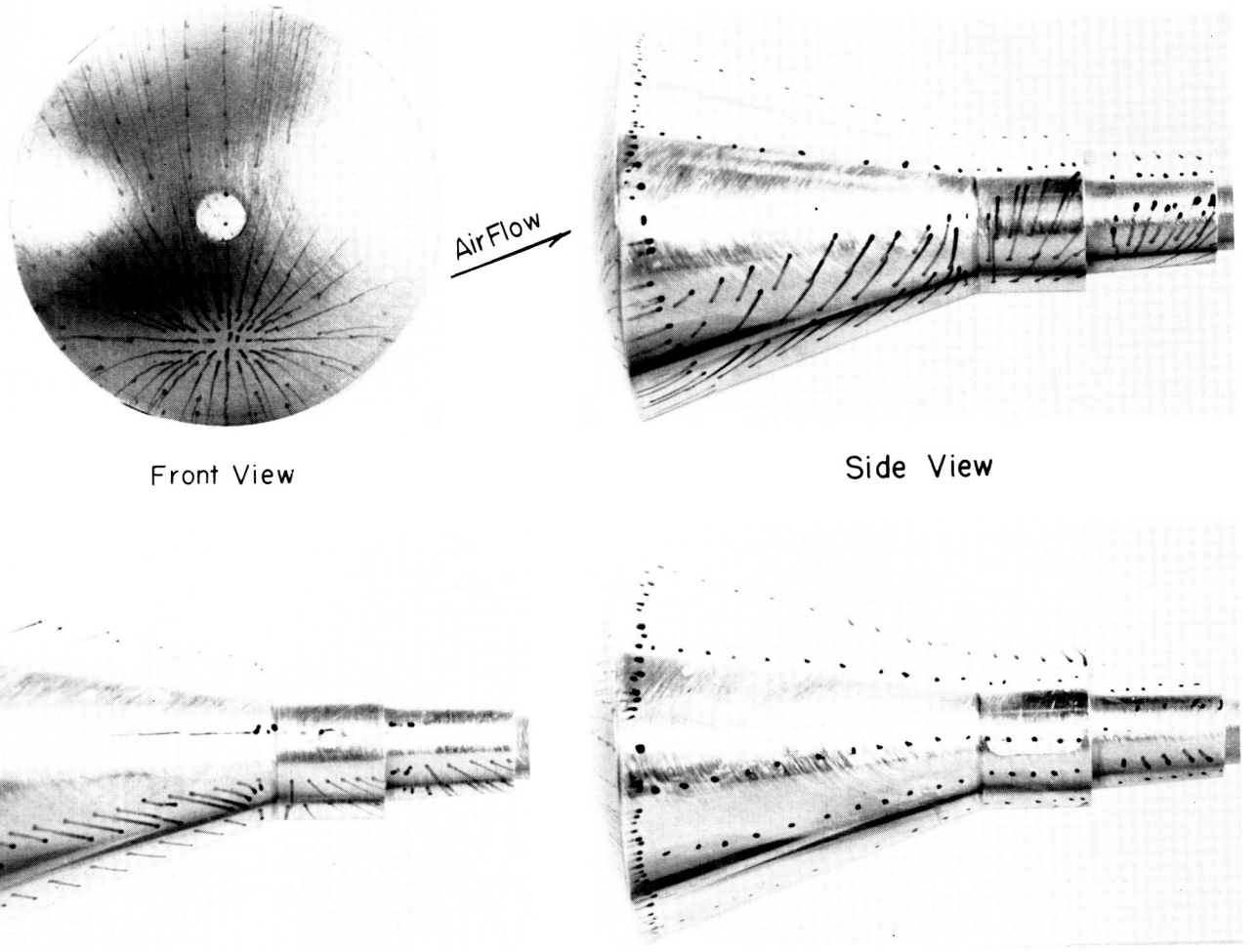

(e) $\alpha = 20^{\circ}$. L-60-6976

Figure 8.- Concluded.

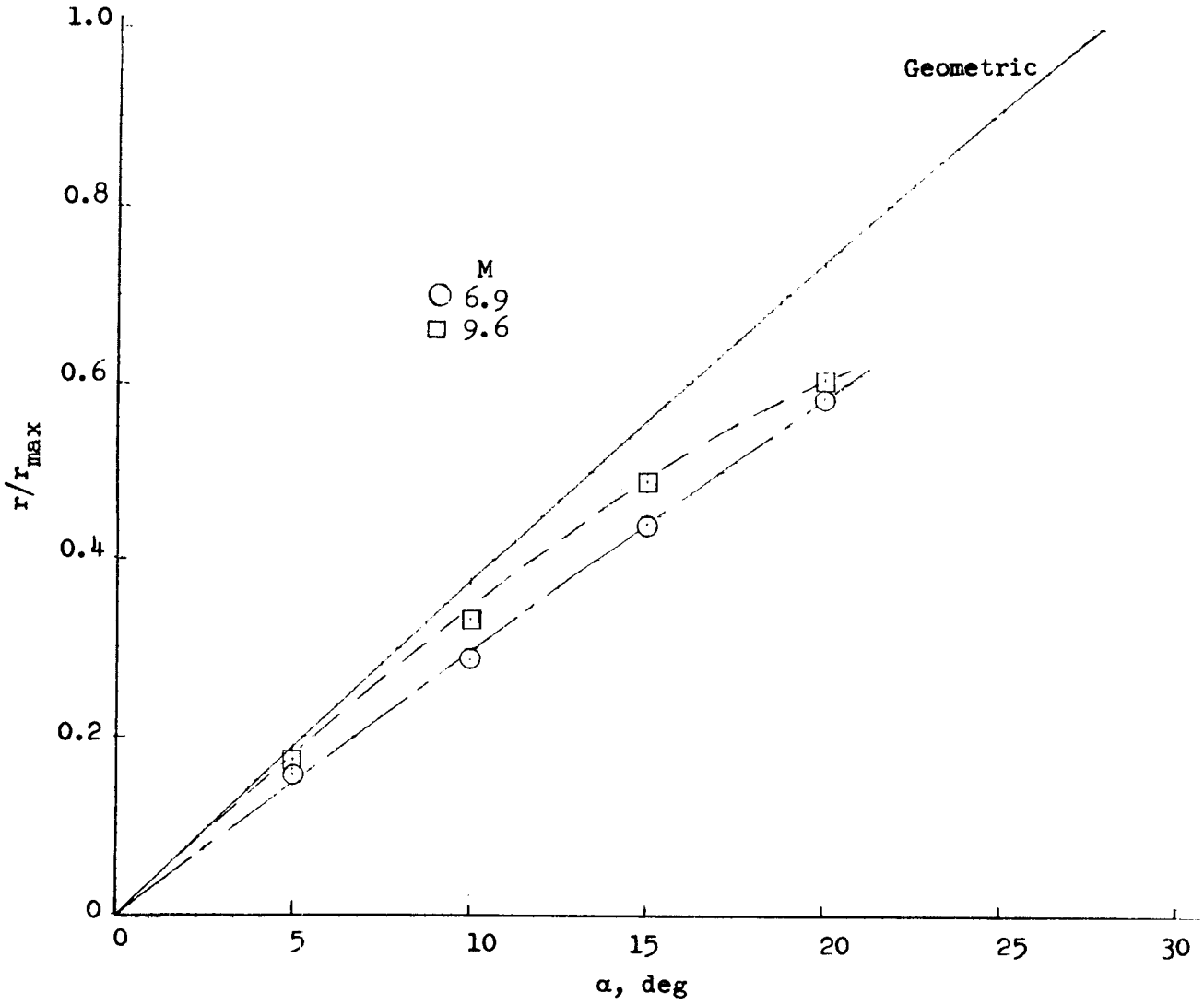

Figure 9.- Variation of stagnation-point location with angle of attack.

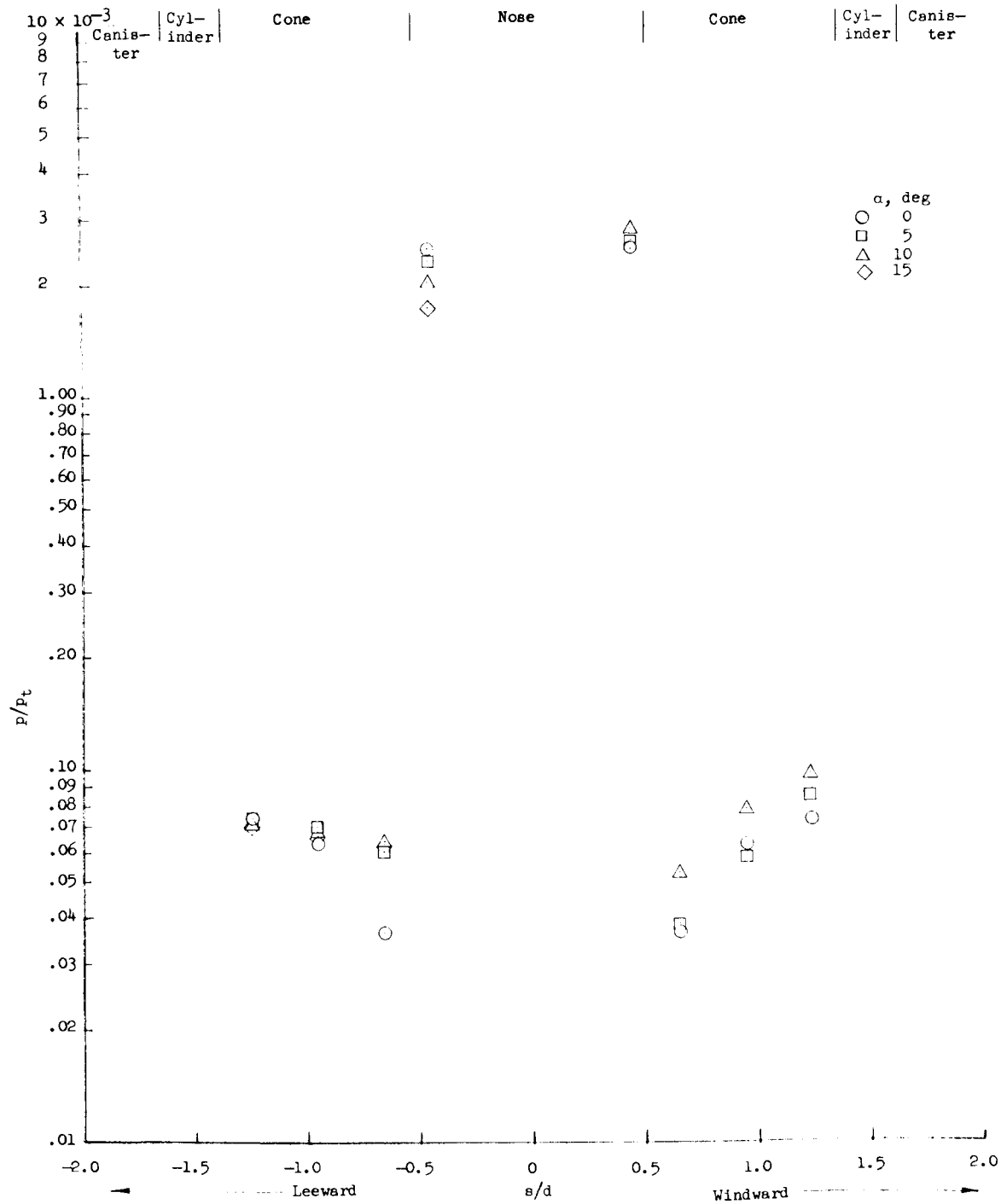

(a) $\phi = 0^{\circ}$.

Figure 10.- Pressure distribution along the capsule. M = 9.6.

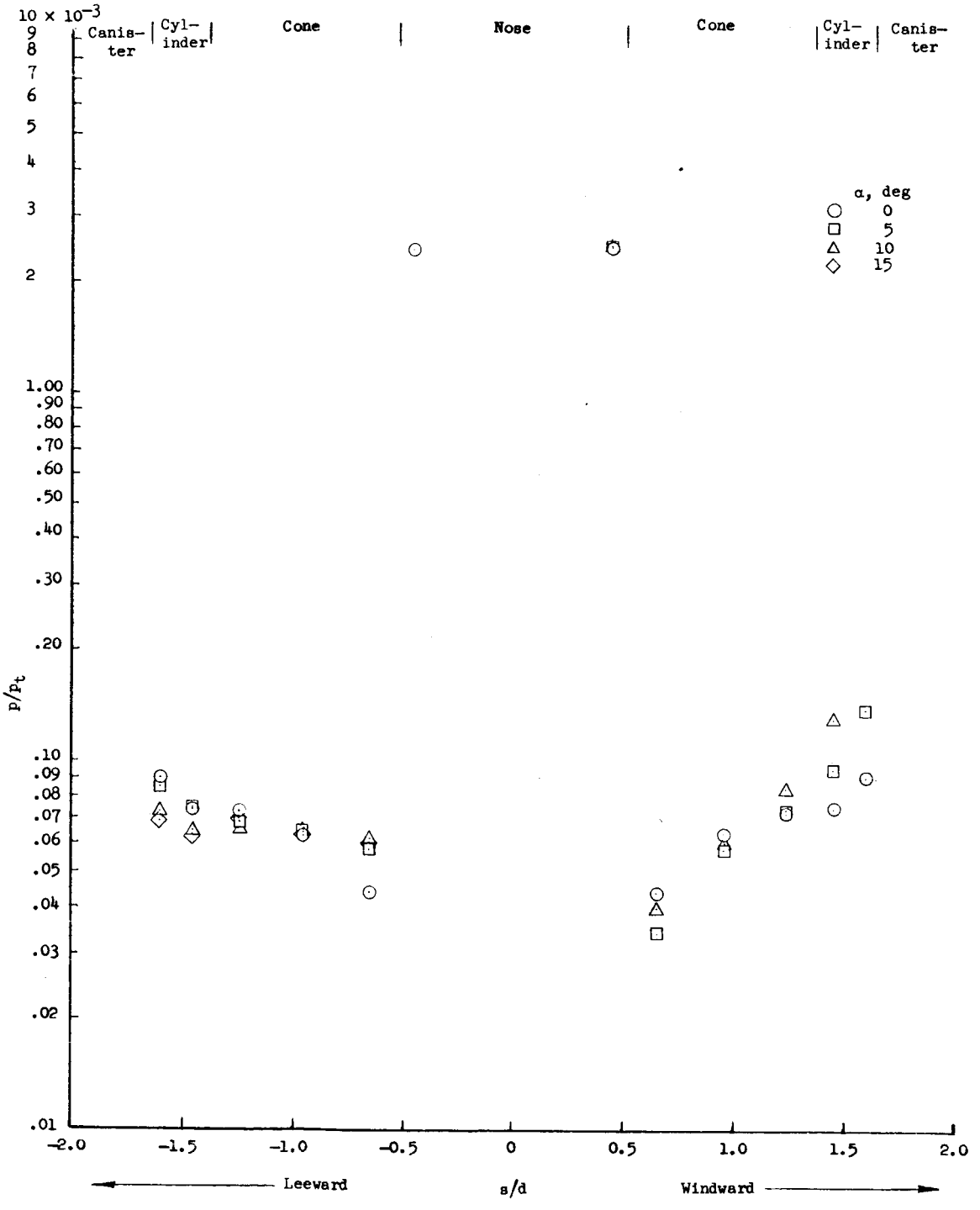

(b) $\phi = 45^\circ$.

Figure 10.- Continued.

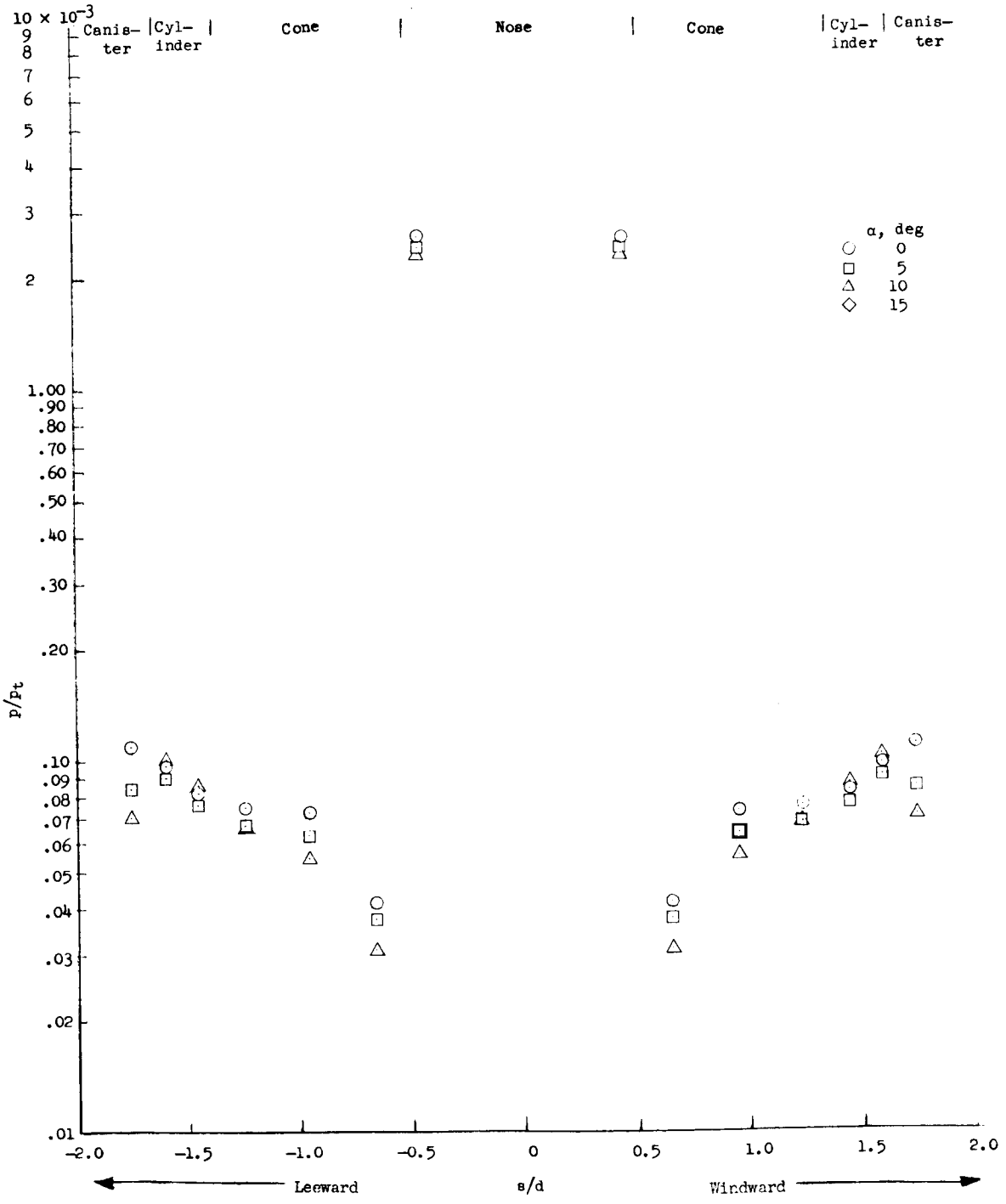

(c) $\phi = 90^{\circ}$.

Figure 10.- Concluded.

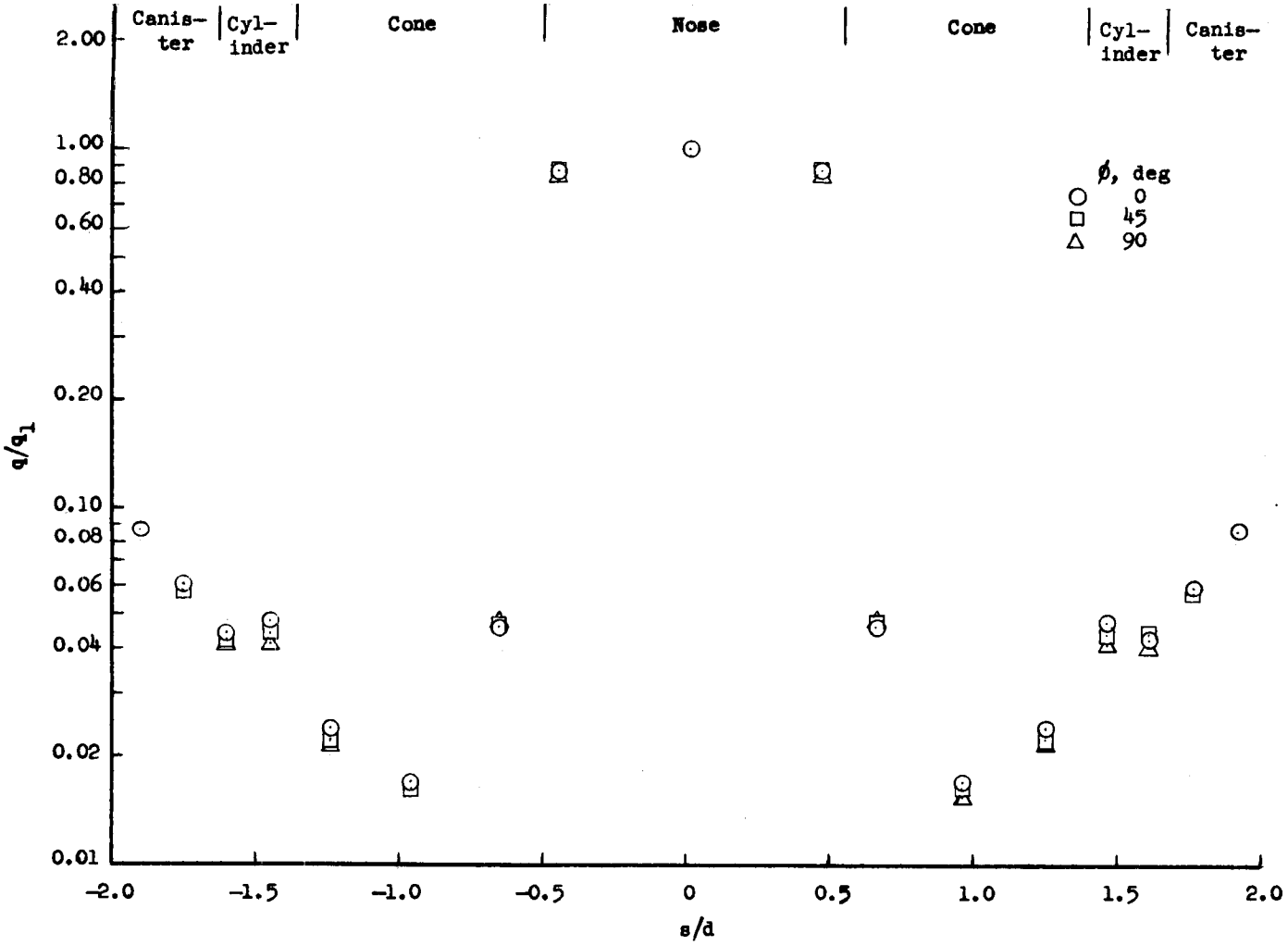

(a) $\alpha = 0^{\circ}$.

Figure 11.- Distribution of heat-transfer rates along body. M = 9.6.

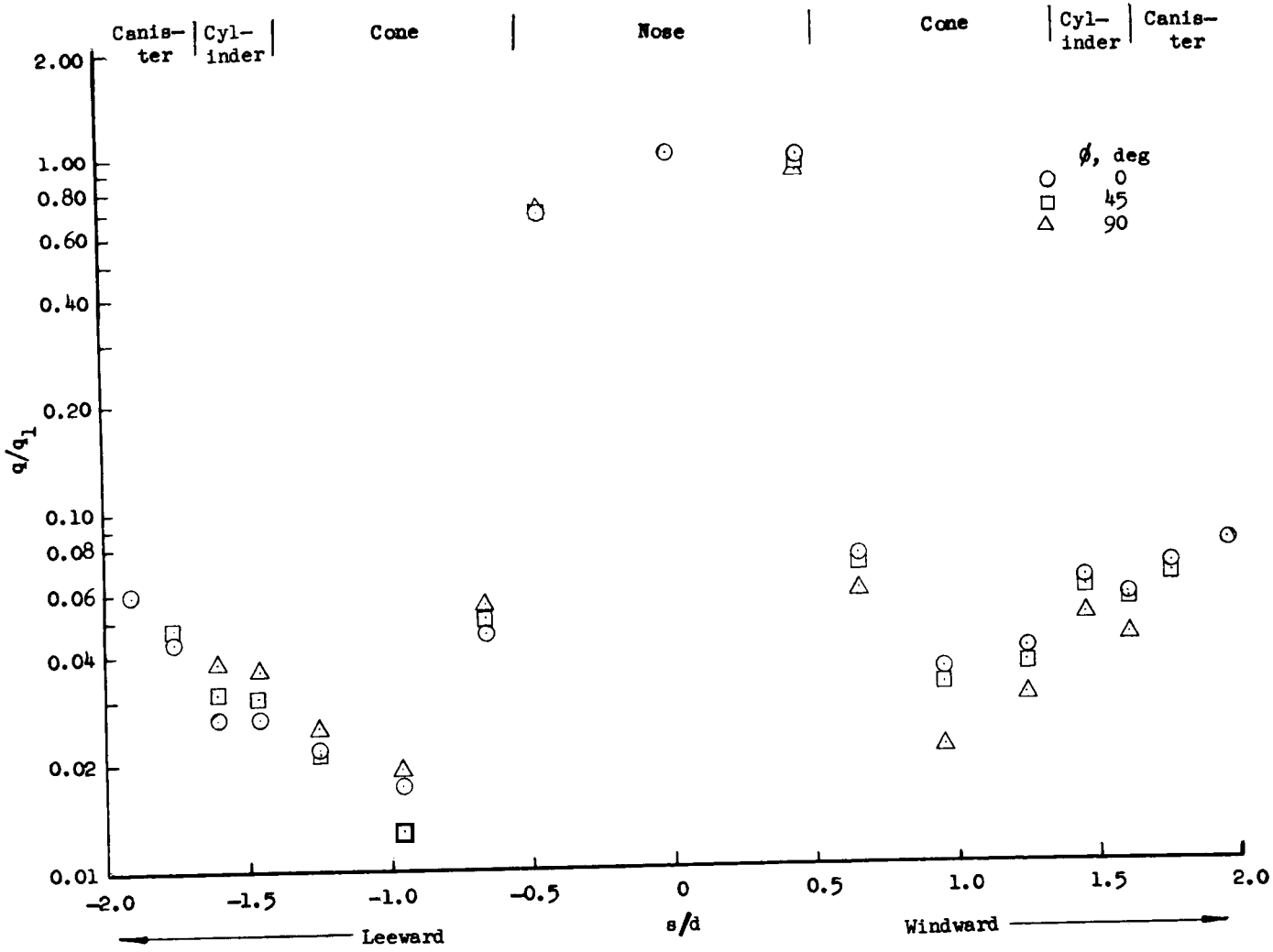

(b) $\alpha = 5^{\circ}$.

Figure 11.- Continued.

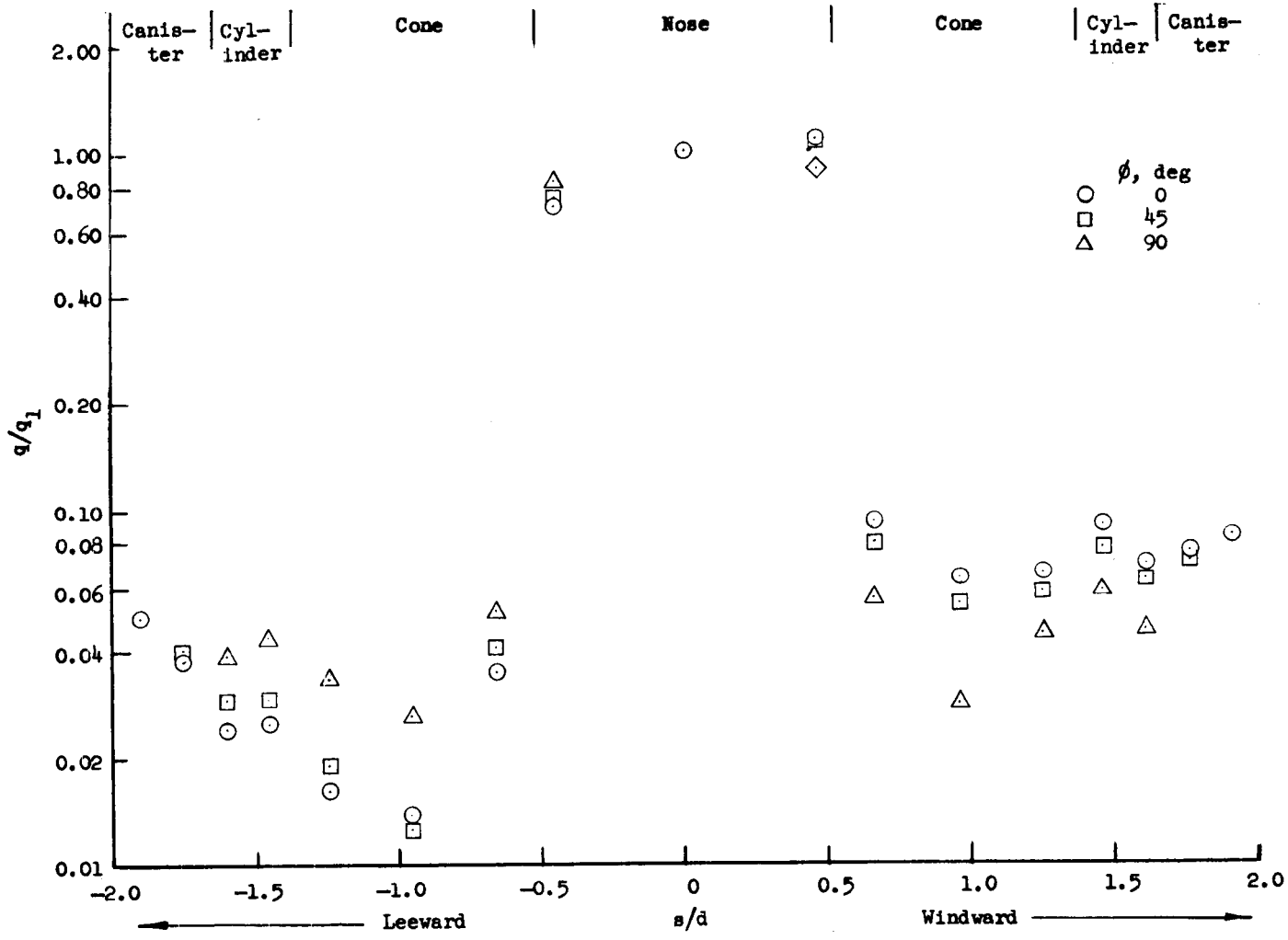

(c) $\alpha = 10^{\circ}$.

Figure 11.- Continued.

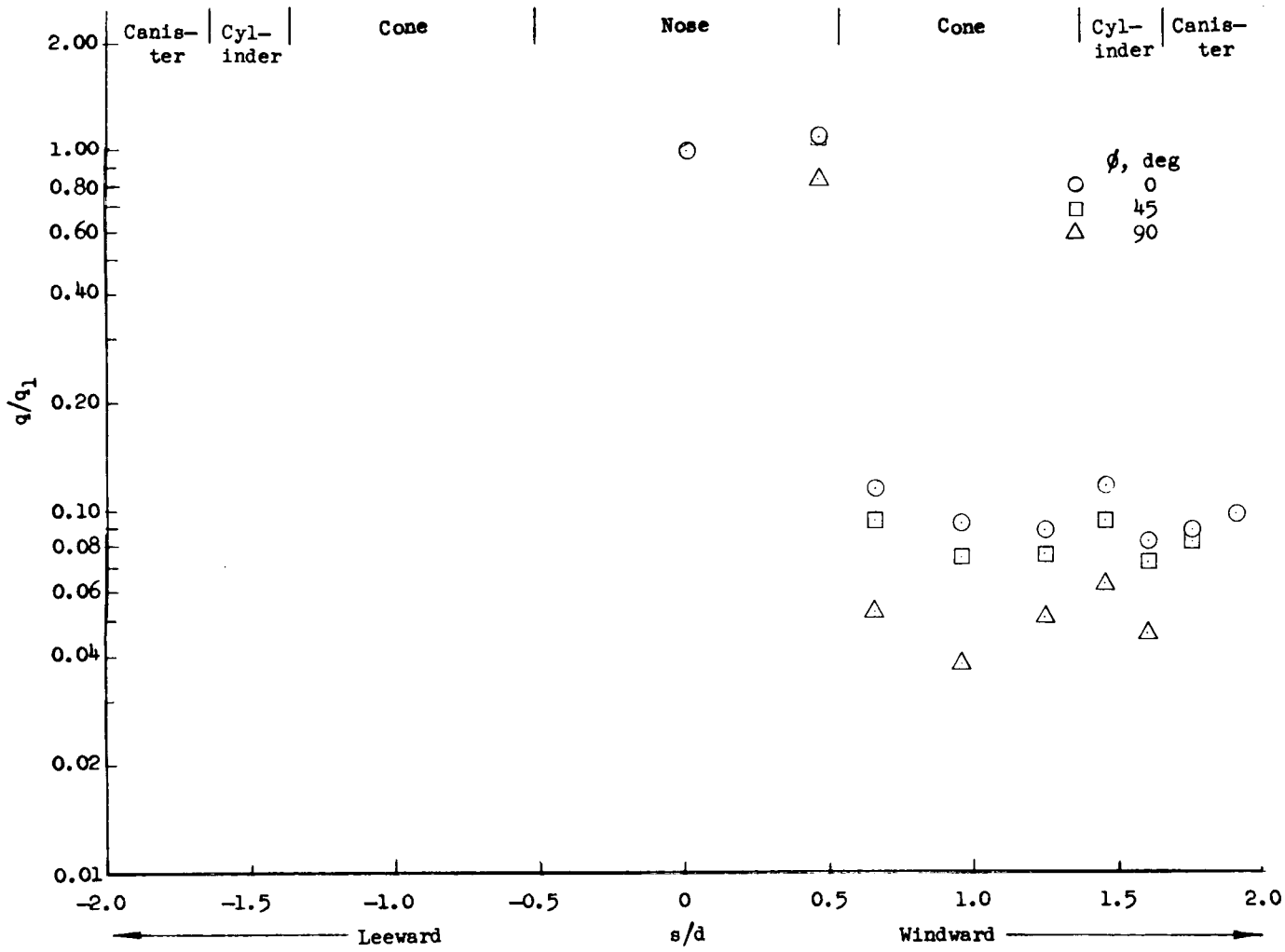

(d) $\alpha = 15^{\circ}$.

Figure 11.- Concluded.

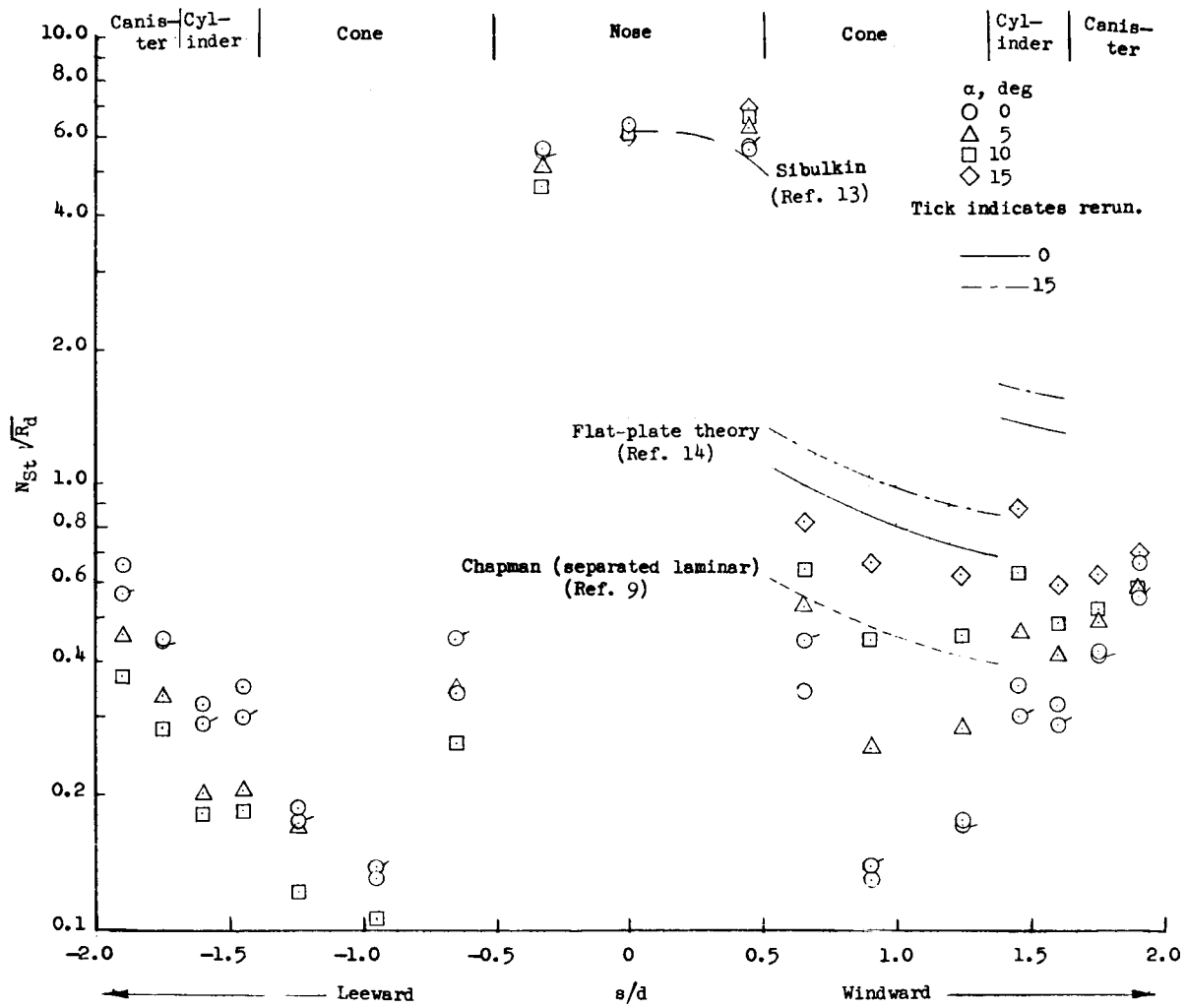

(a) $\phi = 0^{\circ}$.

Figure 12.- Distribution of Stanton number along capsule. M = 9.6.

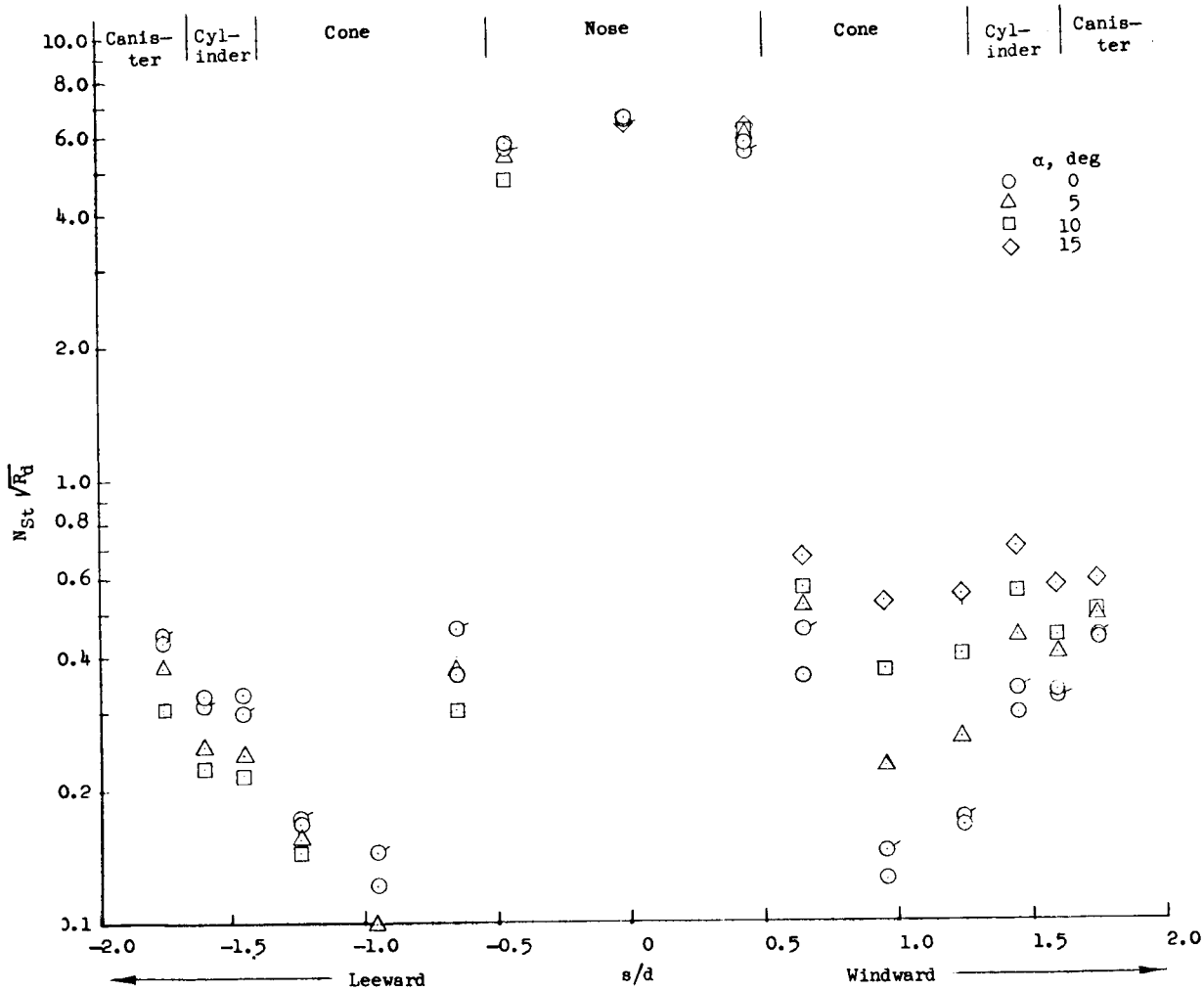

(b) $\phi = 45^{\circ}$.

Figure 12.- Continued.

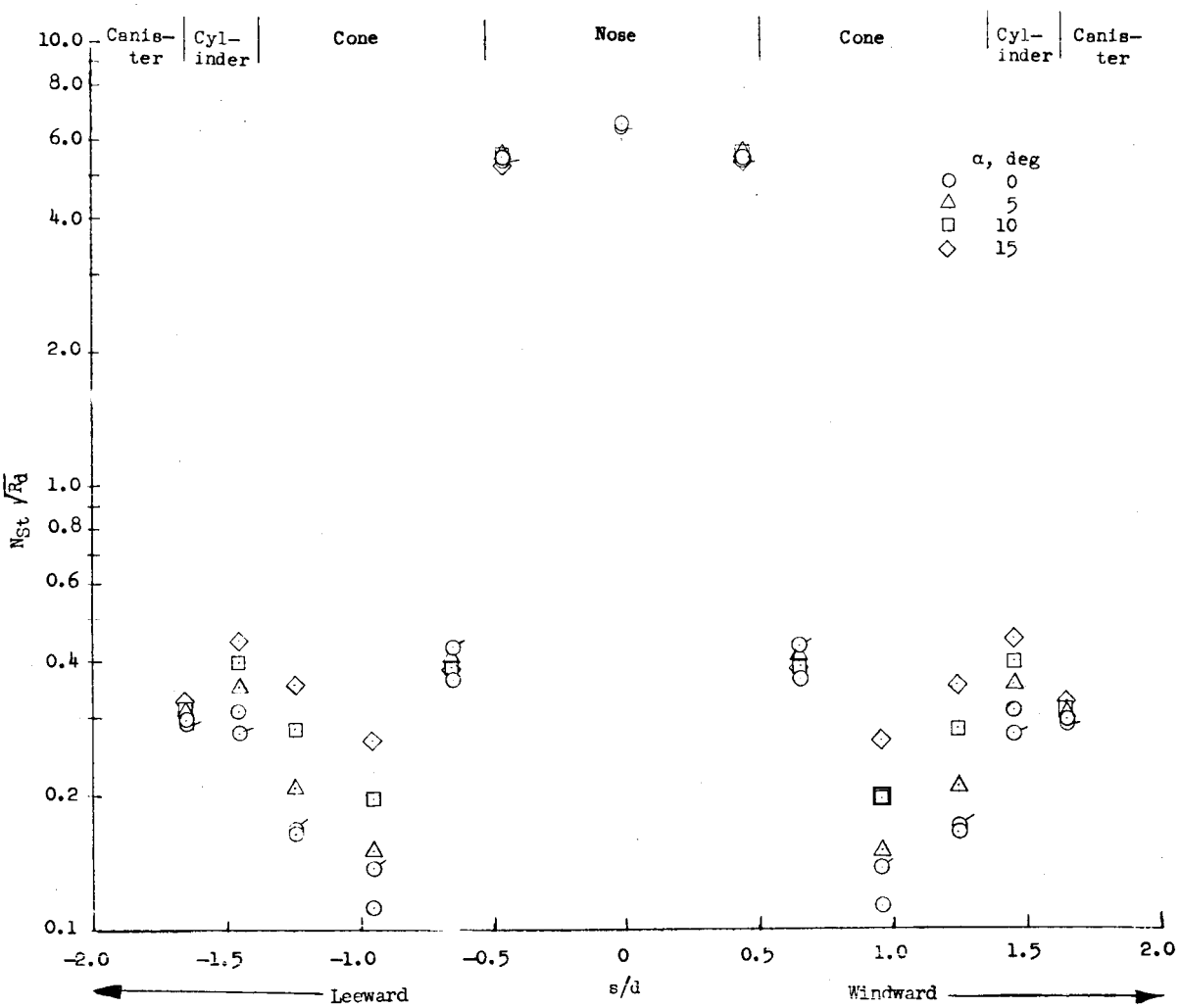

(c) $\phi = 90^{\circ}$.

Figure 12.- Concluded.

[redacted]

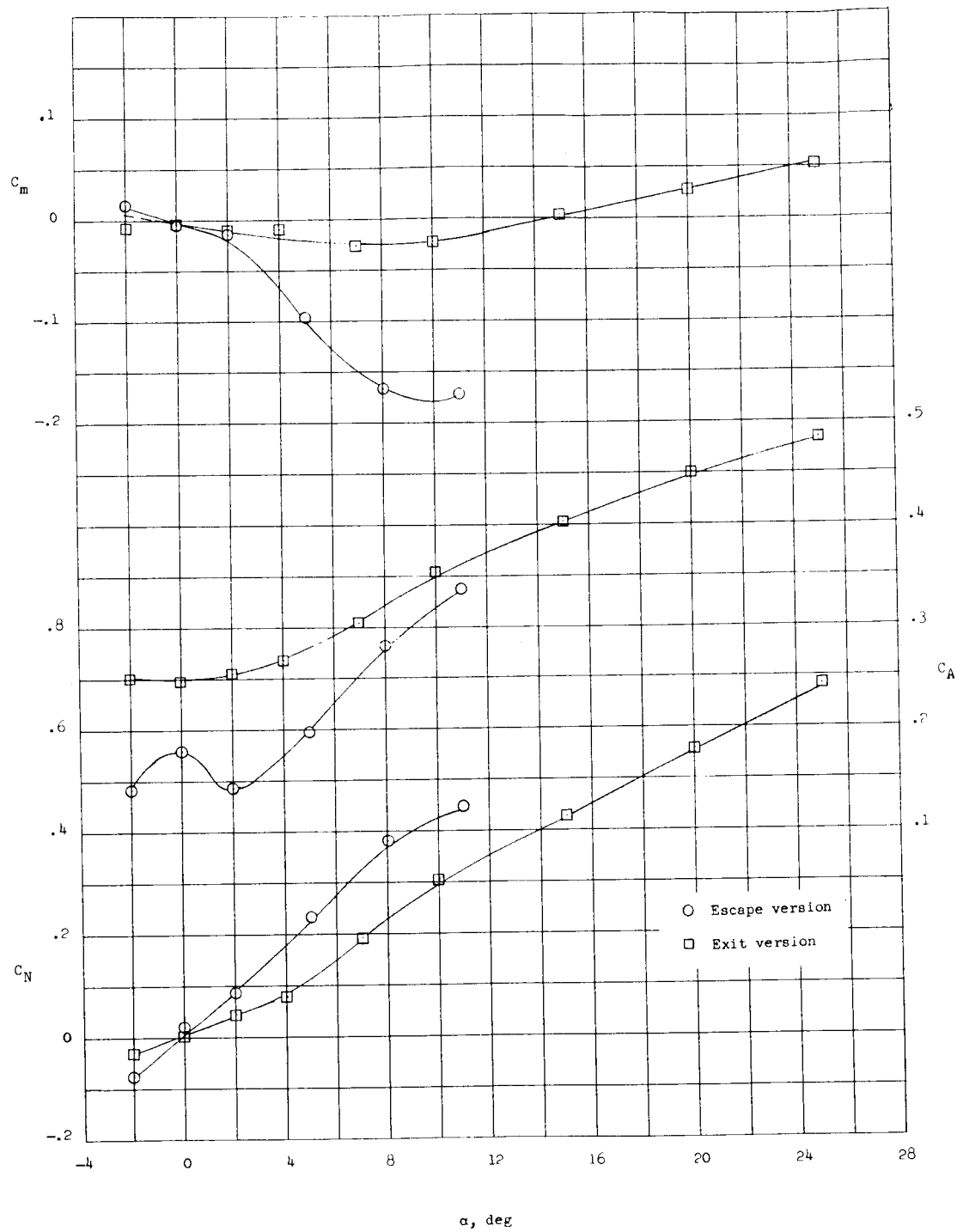

Figure 13.- Aerodynamic characteristics in pitch of escape and exit versions of the Mercury capsule. M = 9.6; R_d = 0.14 × 10^6.

L-1220

[redacted]

B

DECLASSIFIED

L-1220

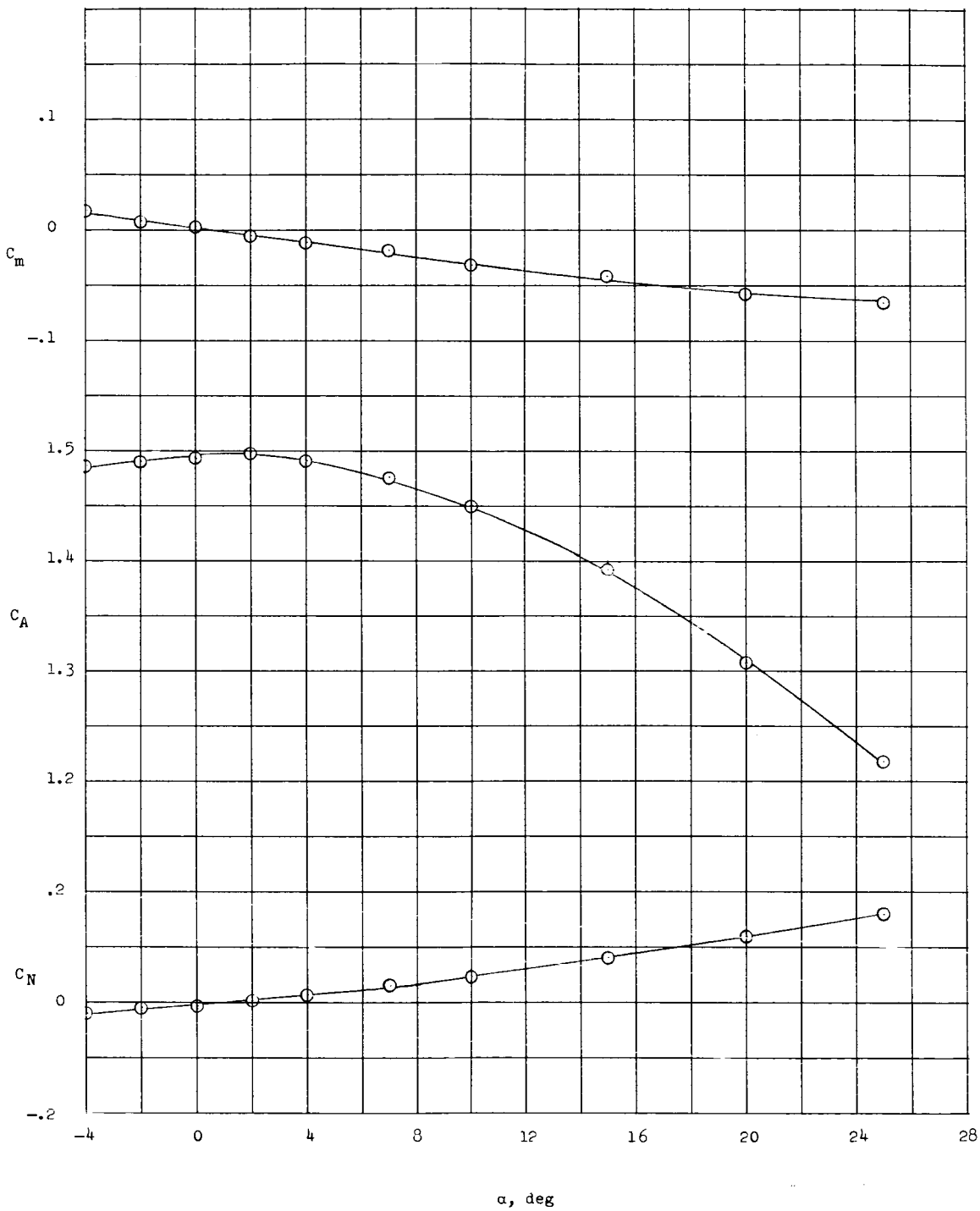

Figure 14.- Aerodynamic characteristics in pitch of reentry version of Mercury capsule. M = 9.6; $R_d = 0.14 \times 10^6$.

[redacted]

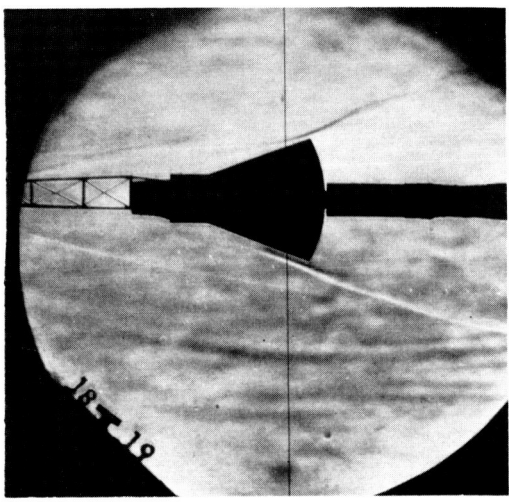

$\alpha = 0^{\circ}$

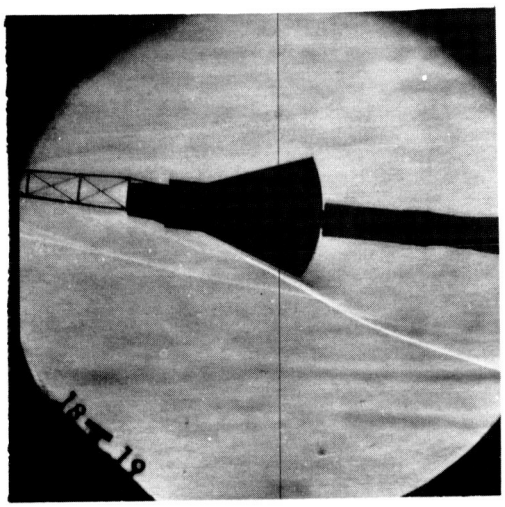

$\alpha = 5^{\circ}$

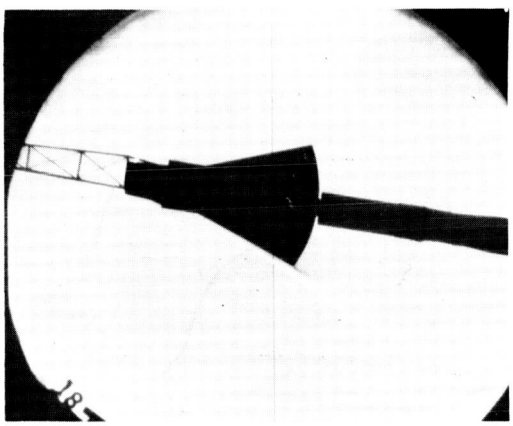

$\alpha = 8^{\circ}$

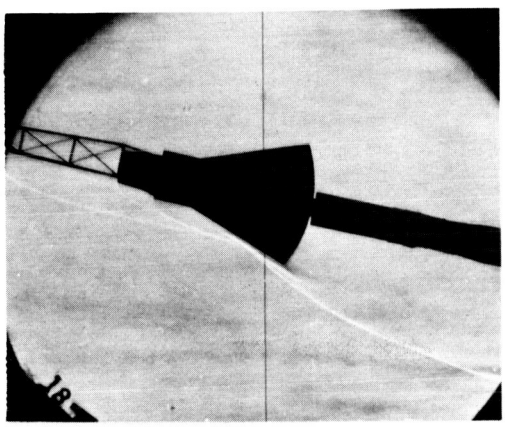

$\alpha = 11^{\circ}$

(a) Escape version. L-60-8305

Figure 15.- Schlieren photographs of Mercury capsule configurations. (Stability tests at M = 9.6.)

L-1220

[redacted]

DECLASSIFIED

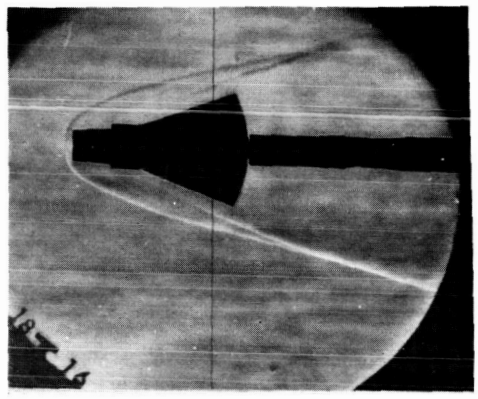

$\alpha = 0^{\circ}$

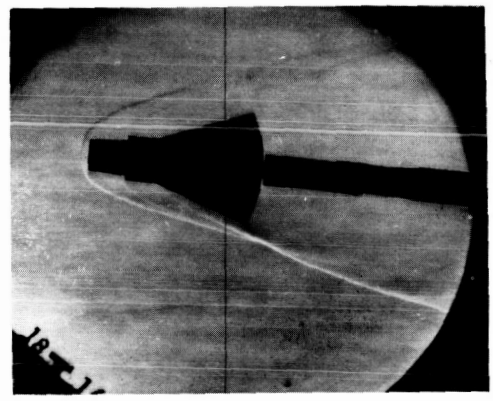

$\alpha = 4^{\circ}$

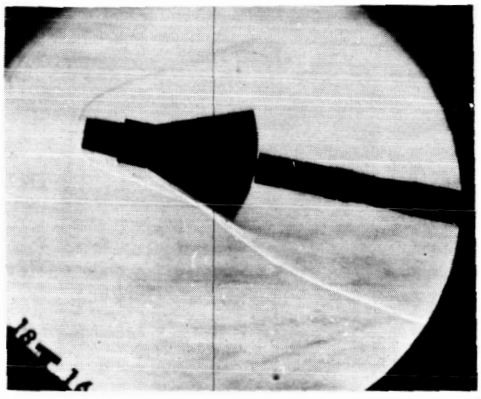

$\alpha = 10^{\circ}$

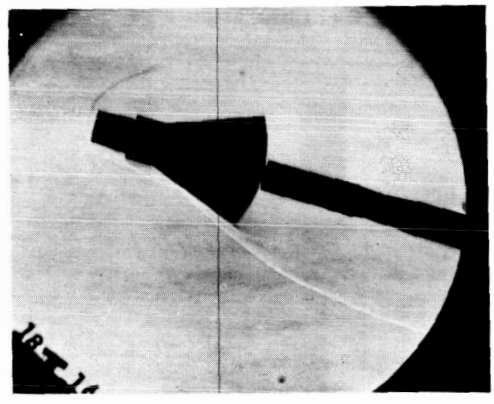

$\alpha = 15^{\circ}$

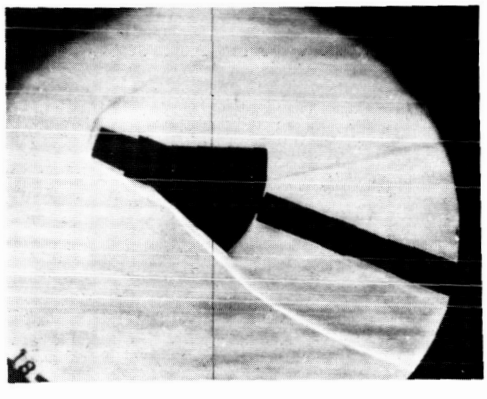

$\alpha = 20^{\circ}$

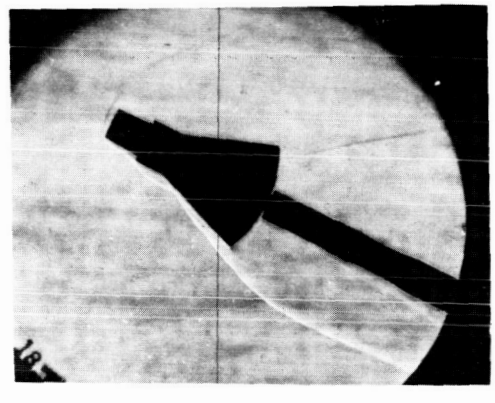

$\alpha = 25^{\circ}$

(b) Exit version. L-60-8306

Figure 15.- Continued.

[redacted]

CONFIDENTIAL

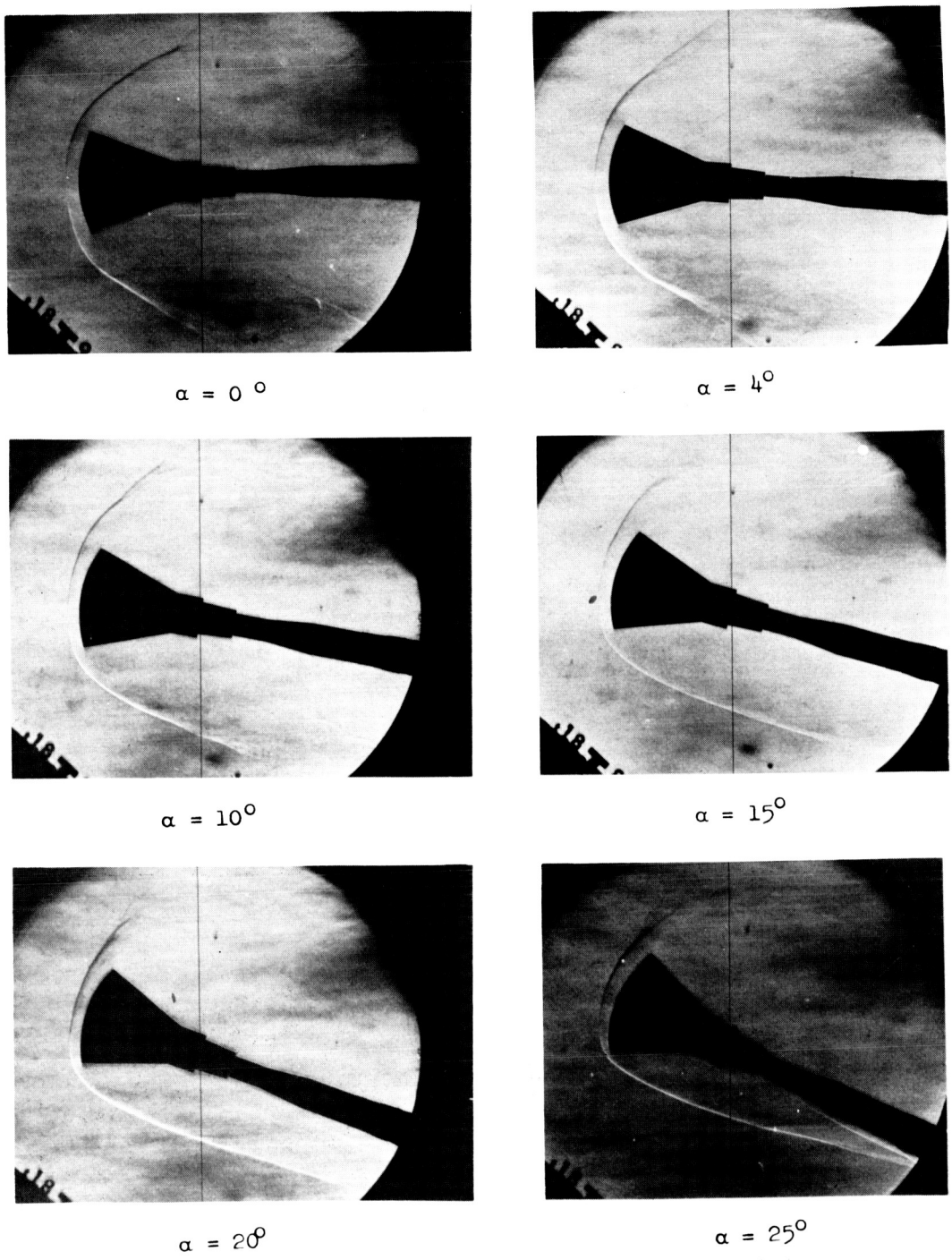

α = 0°

α = 4°

α = 10°

α = 15°

α = 20°

α = 25°

(c) Reentry version. L-60-8307

Figure 15.- Concluded.

NASA - Langley Field, Va. L-1220

L-1220